Toxicology and Applied Pharmacology 404 (2020) 115178

Contents lists available at ScienceDirect

Toxicology and Applied Pharmacology

journal homepage: www.elsevier.com/locate/taap

# Effects of silver nanoparticles on T98G human glioblastoma cells

Encarnación Fuster, Héctor Candela, Jorge Estévez, Ariel J. Arias, Eugenio Vilanova, Miguel A. Sogorb*

*Instituto de Bioingeniería, Universidad Miguel Hernández de Elche, 03202, Elche, Spain*

ARTICLE INFO

*Keywords:*
Silver nanoparticles
Human glioblastoma
Nanotoxicology
T98G cells
*in vitro* transcriptomics
Neurotoxicity

ABSTRACT

Nanotechnology has been well developed in recent decades because it provides social progress and welfare. Consequently, exposure of population is increasing and further increases in the near future are forecasted. Therefore, assessing the safety of applications involving nanoparticles is strongly advisable. We assessed the effects of silver nanoparticles at a non-cytotoxic concentration on the performance of T98G human glioblastoma cells mainly by an omic approach. We found that silver nanoparticles are able to alter several molecular pathways related to inflammation. Cellular repair and regeneration were also affected by alterations to the fibroblast growth factor pathways operating mainly *via* mitogen-activated protein kinase cascades. It was concluded that, given the relevant role of glia on central nervous system maintenance homeostasis, exposure to silver nanoparticles could eventually lead to severe toxicity in the central nervous system, although current exposure levels do not pose a significant risk.

## 1. Introduction

The world around us is formed by blocks of matter of wide-ranging sizes, from small atoms or molecules to much bigger aggregates. Parts of these blocks of matter fall within the so-called nanometric range. The European Commission (EC) defined the term nanomaterial (NM) as a material formed of natural, contaminating or manufactured particles which, in an unbound, aggregate or agglomerate state, contain 50% or more of their particles within the size range between 1 and 100 nm in one of their dimensions or more (EU, 2011). According to this definition, fullerenes, graphene flakes and single-wall carbon nanotubes with one external dimension or more below 1 nm and should also be considered NMs (EU, 2011). Hoyt and Mason (2008) considered NMs with a much simpler definition: those materials with at least one of their dimensions measuring less than 100 nm.

In the last few decades, scientific and engineering development has allowed the manufacture of hundreds of these NMs, which display "smarter" behaviours because they can be, for example, lighter, stronger, harder, more conductive or electromagnetic (among other properties) than their analogous materials on a non-nanometric scale. Certain NMs can also carry drugs coated on their surface, or even exhibit antimicrobial activity themselves. Nanotechnology can be considered one of the greatest scientific advances in the early 21st century and it has been estimated that its economic impact will be around US $75 billion by 2020 (Mulvaney and Weiss, 2016).

The above-stated properties suggest that nanotechnology possesses the capability to bring to society huge progress and welfare and, therefore, the use of NMs should be widespread, with an expected high exposure level for human beings and the environment. Some examples to illustrate this high exposure potential might be: i) the Consumer Products Inventory reported 1814 consumer products from 622 companies in 32 countries (Vance et al., 2015); ii) according to the

*Abbreviations:* ACTI, Scientific and Technical Research Area of University of Murcia; Ag-NP, Silver nanoparticles; DEG, Differentially Expressed Genes; DEP, Diethylpyrocarbonate; DLS, Dynamic Light Scattering; DUSP, DUal Specificity protein Phosphatases; EC, European Commission; EF, Enrichment Factor; EGF, Epidermal Growth Factor; ERK1, Extracellular-signal Regulated Kinase 1; ERK2, Extracellular-signal Regulated Kinase 2; EUON, European Union Observatory for Nanomaterials; FBS, Foetal Bovine Serum; FDR, False Discovery Rate; FGF, Fibroblast Growth Factor; FPKM, Number of fragments sequenced per kilobase of gene and million fragments; FSC, Small angle Forward Scatter; GAPDH, Glyceraldehyde 3-phosphate dehydrogenase; GO, Gene Ontology; IL, Interleukin; IL6, Interleukin-6; IL8, Interleukin-8; JUNB, Transcription factor Jun-B; MAPK, Mitogen Activated Protein Kinase; MTT, 3-(4,5-dimethylthiazol-2-yl)-2,5-diphenyltetrazolium-bromide; NM, Nanomaterial; NPs, Nanoparticles; OECD, Organization for Economic Cooperation and Development; PANTHER, Protein ANalysis THrough Evolutionary Relationships; PBS, Phosphate Buffer Saline; PGK1, Phosphoglycerate kinase 1; RIN, RNA Integrity Number; RNAseq, Massively parallel RNA sequencing; RT-PCR, Real Time quantitative Polymerase Chain Reaction; SEM, Scanning Electron Microscopy; SPRY2, Protein sprouty homolog 2; SPRY4, Protein sprouty homolog 4; SSC, Small angle Side Scatter; STAT, Signal Transducer and Activator of Transcription; TEM, Transmission Electron Microscopy

* Corresponding author.
*E-mail address:* msogorb@umh.es (M.A. Sogorb).

https://doi.org/10.1016/j.taap.2020.115178
Received 14 April 2020; Received in revised form 11 July 2020; Accepted 28 July 2020
Available online 30 July 2020
0041-008X/ 

European Union Observatory for Nanomaterials (EUON), some uses currently considered for NMs include: coatings and paintings, pharmaceutical products, cosmetics and personal care products, plastics and rubber, fabrics, textiles and clothing, sports equipment, and the food industry.

Silver nanoparticles (Ag-NP) are one of the most widely used NMs, whose most recognised uses are: i) textile materials to improve antibacterial finishes (Gokarneshan and Velumani, 2017); ii) biomedical applications (antibacterial, drug-delivery systems, catheter modification, dental applications, wound and bone healing, and others) (Burdușel et al., 2018); iii) cosmetics (bath and shower products, body and external intimate care products, face care masks and other face products, foot care products, make-up remover products, mouth washes, pre- and after-shaving products, products with antiperspirant activity, shampoo, soap products, toothpaste, and other skin products) (EC, 2016).

The proper assessment of the safety of NMs involved in all their expected applications will be a task of enormous complexity and Herculean proportions. Two pieces of information can help us to understand the magnitude of the required effort: 1) the vast variety of chemical compositions, shapes, sizes and coatings for which NMs may be required; 2) the dynamic interactions of NMs with the surrounding environment, for example: i) nanoparticles (NPs) can agglomerate to form aggregates (thus generating new NPs of various sizes and shapes) in different ways depending on the biological fluid containing them; ii) macromolecules (basically lipids and proteins) can be adsorbed on the surface of NPs to generate a new NM that might interact with the surrounding medium in a different way. As a result of the above situations, only a few NMs have been subjected to detailed toxicological studies to date. Research work has focussed mainly on those with a high exposure potential for which there is evidence to suggest that they may cause adverse effects on human health or the environment. Based on these criteria, the Organization for Economic Cooperation and Development (OECD) drew up a list of NMs whose security should be assessed as a priority (OECD, 2010), including, among others, the Ag-NP herein used.

Several *in vivo* toxicological Ag-NP assessments in animal models have shown adverse effects, such as genotoxicity, inflammation in lungs and liver, hepatotoxicity and cytogenetic disorders in colon, but not neurotoxicity (Rezvani et al., 2019). Węsierska and co-workers (2018) concluded that the memory impairment induced by the oral administration of Ag-NP to rats should be attributed to silver ions rather than to NPs. However, certain issues cause concern about the capability of Ag-NP to induce neurotoxicity, such as: i) evidences suggesting that Ag-NP can be translocated from blood to the brain (Strużyńska and Skalska, 2018); ii) *in vitro* experiments describing impairments in the performance of glutaminergic neurons and astrocytes derived from human embryonic stem cells (Begum et al., 2016; Repar et al., 2018); iii) *in vivo* apoptosis in rat hippocampal cells induced after repeated intraperitoneal injection (Ghooshchian et al., 2017).

It is estimated that glia cells represent around 80% of the cells in the human brain and are actively involved in the homeostasis of the central nervous system by participating in the vast majority of neurobiological processes (Barres et al., 2015). This converts these cells in a very interesting model to study the neurotoxicity of NPs, as impairments in the performance of glia cells can lead to impairments in blood brain barrier integrity, neural plasticity and myelination, or can trigger the development of neurodegenerative diseases. It is also noted that information about the effects of Ag-NP on glia is quite scarce; thus, we decided to study the potential neurotoxicity of Ag-NP on glial cells in this work.

We have used a transcriptomic approach to determine the effects of Ag-NP on the performance of T98G human glioblastoma cells at doses that exert low cytotoxicity. Several biological processes were altered by Ag-NPs, of which the most relevant were the inflammation response and the fibroblast growth factor (FGF) receptor-signalling pathway. The latter operated mainly through mitogen-activated protein kinase (MAPK) cascades.

## 2. Material and methods

### 2.1. Silver nanoparticles

Ag-NPs capped with citrate, with an average diameter of 10 ± 6 nm (catalogue number AG-00, batch 16,002), were provided by SCHARLAB (www.scharlab.com) in sterile milli-Q water at 1 mg/ml. This 1 mg/ml yellow suspension was sonicated for 10 min at 110 W in a water bath before preparing a 400 μg/ml stock solution in phosphate buffer saline (PBS). This stock solution was stored at 4 °C in the dark.

Ag-NPs suspensions at appropriate concentration were prepared in fresh cell culture medium immediately before cellular exposures began. To this end, the 400 μg/ml stock solution was re-sonicated as described above, and the required aliquots were added to the appropriate cell culture medium volume.

### 2.2. Physico-chemical characterisation of Ag-NPs

The supplier provided the transmission electron microscopy (TEM) image shown in Supplementary Material Fig. 1A and the UV-VIS absorbance spectrum displayed in Supplementary Material Fig. 1B. Silver Ag-NPs displayed a maximum absorbance between 550 and 600 nm. We requested an additional physical characterisation of the Ag-NPs batch from Nanoimmunotech SL (https://nanoimmunotech.eu/en), which included the parameters described below.

#### 2.2.1. Particle size in water by dynamic light scattering (DLS)

Measurements were taken by Malvern Zetasizer ZS equipment at 25 °C. Ag-NPs were diluted in type 1 water (18 MΩ.cm) and were analysed by quintuplicate with a minimum of 10 runs per measurement.

#### 2.2.2. Z-potential in water

Measurements were taken by Malvern Zetasizer ZS equipment at 25 °C. Ag-NPs were diluted in type 1 water (18 MΩ.cm) and were analysed by triplicate after adjusting the number of runs to the specific necessity of each sample.

#### 2.2.3. Transmission electron microscopy

Samples were placed on copper grids with a carbon film and were air-dried. Images were taken using a TECNAI F30 (300 kV) microscope and were further processed with the ImageJ free software.

#### 2.2.4. Stability of Ag-NPs in cell culture medium

Suspensions of Ag-NPs were prepared in RPMI cellular medium supplemented with 10% foetal bovine serum (FBS) and in type I water. These suspensions were incubated at 37 °C. Particle size was determined by DLS, as described above, after 0, 24 and 72 h.

### 2.3. Cellular cultures

T98G human glioblastoma cells (catalogue number 92090213) were provided by the European Collection of Authenticated Cell Cultures (https://www.phe-culturecollections.org.uk/collections/ecacc.aspx). According to the provider, these cells derive from a glioblastoma multiform tumour from a 61-year-old Caucasian male.

Cells were grown and expanded until confluence using P100 TPP plates in Dulbecco's modified Eagle Medium-GlutaMAX™-I with 1 g/l glucose and 110 g/l sodium pyruvate supplemented with 10% FBS and 1% non-essential amino acids (750 mg/l glycine +890 mg/l L-alanine +1320 mg/l asparagine +1330 mg/l aspartic acid +1470 mg/l glutamic acid +1150 mg/ml proline +1050 mg/ml serine) and 1% penicillin (10,000 U/ml), plus streptomycin (10,000 U/ml). Cells were cultured at 37 °C in a 5% $CO_2$ atmosphere.

Having reached confluence, cells were sub-cultured in either P60 TPP plates or 96-well trays at the appropriate density according to the specific experiment. For this purpose, the cell culture medium used for cell growth and expansion were removed from the plates. Then cells were washed twice with PBS. Afterwards, a solution of 0.25% Trypsin/0.53 mM EDTA was added and cells were left for 3 min in the $CO_2$ incubator. Trypsin action was stopped by adding an equal volume of complete cell medium and cells were dispersed by gently pipetting. Finally, the resulting cellular density was determined using trypan blue and a Neubauer cell-counting chamber, and the samples were concentrated or diluted if necessary until the cell density needed to start each specific experiment was reached.

### 2.4. Cellular exposure to Ag-NPs

Cells were seeded in suitable trays at appropriate densities on experiment day 0 and were incubated in complete medium at 37 °C and in a 5% $CO_2$ atmosphere for 24 h. On day 1, the cell culture medium was removed. Afterwards, fresh culture medium containing appropriate concentrations of Ag-NPs was added to cells and an appropriate exposure time was allowed (72 h in most cases).

### 2.5. Cellular viability tests

Certain studies suggest that not all viability tests are appropriate for all NPs (Monteiro-Riviere et al., 2009; Kroll et al., 2012). Thus, cellular viability after exposure to Ag-NPs was assessed by two different tests: (i) the 3-(4,5-dimethylthiazol-2-yl)-2,5-diphenyltetrazoliumbromide (MTT) test, which addresses mitochondria as the toxicity target; and (ii) the neutral red uptake test, which addresses the lysosome as the toxicity target.

Each experimental condition was assayed (for both tests) during each independent experiment with six biological replicates (6 different wells of the same culture in the same tray). The MTT test involved nine independent experiments (they were all performed with independent cultures), while the neutral red test involved seven independent experiments. In all cases, the percentage of viability of the cell cultures exposed to Ag-NPs was estimated by assuming as 100% viability the absorbance of the control cultures (not exposed to Ag-NPs). In all the experiments, the cytotoxicity-positive controls were run using 10 μg/ml of $CuSO_4$, which was able to reduce the viability of the exposed cultures by around 80%.

#### 2.5.1. MTT test

T98G human glioblastoma cells were exposed in 96-wells plates (5000 cells/plate seeded on day 0) to Ag-NPs. At the end of the 72 h exposure period, Ag-NPs were removed and cells were washed with PBS. Afterwards, 200 μl/well of a 1 mg MTT/ml solution (prepared in 60% (*v*/v) minimum essential medium plus 20% (v/v) FBS) were added and cells were kept at 37 °C in a 5% $CO_2$ atmosphere for 3 h. After this time, the MTT solution was removed and discarded, and cells were washed with PBS. At the end of the process, cells were treated and shaken at room temperature for 10 min with 100 μl/well of dimethyl sulfoxide for lysis. Finally, absorbance at 570 nm was determined and was corrected for the non-specific absorption with absorbance at 690 nm.

#### 2.5.2. Neutral red uptake test

Tests were performed using the Neutral Red Cell Cytotoxicity Assay Kit provided by Biovision (product number K 447). T98G human glioblastoma cells were exposed in 96-wells plates (10,000 cells/plate seeded on day 0) to Ag-NPs. At the end of the 72 h exposure period, Ag-NPs were washed with washing solution. Afterwards, 150 μl/well of neutral red solution were added and cells were kept at 37 °C in a 5% $CO_2$ atmosphere for 2 h. After this time, the neutral red solution was removed and discarded, and cells were washed with washing solution. At the end of the process, cells were treated and gently shaken at room temperature for 20 min with 150 μl/well of the solubilisation solution. Finally, absorbance at 540 nm was determined and it was corrected for the non-specific absorption with absorbance at 690 nm.

### 2.6. Flow cytometry

Flow cytometry services were provided by the Scientific and Technical Research Area of the University of Murcia (Spain) (ACTI) (https://www.um.es/web/acti/). A FACSCanto flow cytometer (Becton Dickinson), equipped with an Ar laser of 488 nm and 20 mV and a He laser of 633 nm and 17 mV, was employed. T98G human glioblastoma cells were exposed in P60 TPP plates (300,000 cells/plate seeded on day 0) to Ag-NPs. Afterwards, Ag-NPs were removed and cells were washed with PBS and detached from the plates with trypsin, as described in Section 2.3, to be further processed as described below according to the scope of the experiment.

#### 2.6.1. Light scattering cytometry

After detachment, cells were re-suspended in PBS at a density of 600,000 cells/ml and transported in an ice bath to the ACTI facilities at the University de Murcia, where they passed through the cytometer that was set up to logarithmically measure the small-angle forward scatter (FSC) intensity (approx. 0–5°) and side scatter (SSC) intensity (approx. 85–95°) of 20,000 events. This technique has been reported to be suitable for studying the uptake of $TiO_2$ NPs (Zucker et al., 2010; Zucker and Daniel, 2012) and other metal NPs (Zucker et al., 2016) in cell cultures. Two independent experiments were performed with two biological replicates per experimental condition in each experiment.

#### 2.6.2. Cell viability

After cell detachment, cells were pelleted (10 min × 850 rpm at 4 °C) and 600,000 cells were re-suspended in 1 ml of cold PBS. They were carried in an ice bath to the ACTI facilities where propidium iodide was added to the mixture, which was further incubated at room temperature for 5 min before placing cells in the cytometer. Each experimental condition was assayed in two independent biological samples.

### 2.7. Electronic microscopy

The electronic microscopy services were provided by ACTI. T98G human glioblastoma cells were exposed in P60 TPP plates (300,000 cells/plate seeded on day 0) to Ag-NPs. Afterwards, Ag-NPs were removed and cells were washed with PBS before being detached from plates with trypsin, as described in Section 2.3. At the end of the 72 h exposure period, Ag-NPs were removed, and 1000,000 cells were pelleted by centrifugation (10 min × 1000 rpm at 4 °C) and re-suspended with 100 μl of fixative solution (3% glutaraldehyde in 0.1 M cacodylate buffer, pH 7.4). Cells were maintained in this state first for 5 min at room temperature and then for 1 h at 4 °C before removing the fixative solution and re-suspending cells with 8% sucrose in 0.1 M cacodylate buffer pH 7.4. In this state, cells were carried in an ice bath to the ACTI facilities, where were treated as described below depending on the scope of the experiment. Two independent experiments with two biological replicates per experimental condition in each experiment were performed for the TEM analysis. One experiment with two biological replicates per experimental condition was performed for the scanning electron microscopy (SEM) analysis.

#### 2.7.1. Transmission electron microscopy

For TEM, samples were treated with 1% osmium tetroxide for 2.5 h at 4 °C. Then cells were washed with 0.1 M cacodylate buffer (pH 7.4) for 12 h and dehydrated with successive 50-min treatments at room temperature with 30%, 50%, 70% and 90% ethanol. The last dehydration step involved a 50-min treatment (twice) with absolute ethanol

and copper sulphate. After dehydration, samples were treated twice with propylene oxide for 15 min before starting the following treatments with Epon (epoxy embedding medium) at room temperature: i) Epon with propylene oxide (1:2) for 45 min; ii) Epon with propylene oxide (1:1) for 2 h; iii) Epon with propylene oxide (2:1) for 2 h; iv) pure Epon overnight. Blocks were finally dried at 70 °C for 48 h before being contrasted with uranyl acetate and lead citrate, sectioned using a Leica UC6 ultra-microtome and analysed with a JEOL JEM-1011 transmission microscope at 80 kV acceleration. Images were captured by a GETTAN BIOSCAN digital camera.

#### 2.7.2. Scanning electron microscopy

For SEM, samples were treated with 1% osmium tetroxide for 2.5 h at 4 °C. Afterwards, cells were washed with 0.1 M cacodylate buffer (pH 7.4) for 12 h and dehydrated with successive 10-min treatments at room temperature with 30%, 50%, 70%, 90% and 100% acetone. Samples were further dried by the critical point methodology and gold-coated. Finally, samples were analysed with the JEOL 6100 scan microscope at 15 kV.

### 2.8. RNA isolation

T98G human glioblastoma cells seeded on day 0 at 160,000 cells/plate in P60 TPP plates were exposed to Ag-NPs. At the end of the 72 h exposure period, Ag-NPs were removed and 1 ml of Trizol Reagent was added to the cells cultured in P60 plates. The culture was gently pipetted to complete cell lysis before transferring the lysate to Eppendorf tubes, which were left for 5 min at room temperature. Afterwards, 0.2 ml of chloroform/ml Trizol Reagent was added to the lysate and this mixture was vigorously shaken for 15–20 s and left again for 5 min at room temperature before centrifuging the samples at 12,000 g and 4 °C for 15 min. This centrifugation separated the organic from the aqueous layer and the latter (containing RNA) was transferred to a new tube. RNA was then precipitated by adding 0.5 ml of isopropanol/ml Trizol Reagent used for lysis and incubating the mixture at −20 °C for 10 min. RNA was collected by centrifugation (12,000 *g* for 15 min at 4 °C) and the pellet was re-suspended with 1 ml of 75% ethanol/ml Trizol Reagent used for lysis and left at −20 °C for 2 days. RNA was collected through centrifugation (7500 *g* for 5 min at 4 °C) and the pellet was allowed to dry before being re-suspended in 0.1% diethylpyrocarbonate (DEPC) nuclease-free water. Each experimental condition was assayed in triplicate (three independent plates of the same culture).

### 2.9. Massively parallel RNA sequencing

T98G human glioblastoma cell cultures seeded on day 0 at 160,000 cells/plate in P60 TPP plates were exposed to Ag-NPs. Afterwards, the RNA of the resulting cultures was isolated as described in Section 2.8. The quality of the resulting preparations was assessed by determining the RNA integrity number (RIN) using Bioanalyzer 2000 (Agilent). Only those samples with a minimum RIN of 7 were considered apt for the massively parallel RNA sequencing (RNAseq) experiments. Libraries were prepared with the TruSeq Stranded mRNA LT Sample Prep kit, and three biological replicates per experimental condition were sequenced by MACROGEN Inc. (https://dna.macrogen.com/eng/) with the Illumina platform using paired-end 101-bp reads.

The RNAseq raw data have been deposited in the NCBI Sequence Read Archive (SRA) (https://www.ncbi.nlm.nih.gov/sra/) with accession number SAMN13151876.

### 2.10. Bioinformatic analysis

The obtained nucleotide sequences were processed with different computer programs. Firstly, the reads were processed with Trimmomatic v. 0.36 software (Bolger et al., 2014) to trim low quality bases and any remaining adapter sequence. The read pairs were then mapped to the GRCh38 version of the human reference genome (Guo et al., 2017) using Hisat2 v.2.1.0 software (Kim et al., 2015) with the –no-discordant and –rna-strandness RF options. The resulting SAM (Sequence Alignment Map) files were converted to BAM (a compressed binary version of a SAM file) format and sorted using Samtools v.0.1.19 software (Li et al., 2009). Expression level was quantified with Cuffdiff (Cufflinks v.2.2.1 package; Trapnell et al., 2010, 2012). The expression level of each gene were expressed as FPKM (fragments per kilobase of transcript and million fragments). Cuffdiff was also used to perform the statistical comparison of the expression level of each gene between both experimental conditions. The heat map was prepared using Gene Cluster v. 3.0 (Eisen et al., 1998) and was visualized with Java Tree View software (Saldanha, 2004).

#### 2.10.1. Ontological analysis

The Gene Ontology (GO) (Ashburner et al., 2000, The GO Consortium, 2017) (http://www.geneontology.org/) terms of the genes differentially expressed as a consequence of exposure to Ag-NPs were assessed. These genes were scored using the PANTHER (Protein ANalysis THrough Evolutionary Relationships) v. 13.1 Classification System (http://pantherdb.org/). PANTHER was used to assign GO terms to the differentially expressed genes, and to determine the nature of their products and the pathways in which they participate.

### 2.11. Validation of massively parallel RNA sequencing by real-time PCR

The expression level of selected genes identified in the RNAseq experiment were further validated in independent experiments by real-time quantitative polymerase chain reactions (RT-PCR) using the StepOnePlus Real-Time PCR System (Applied Biosystems). For this purpose, the T98G human glioblastoma cells seeded on day 0 at 160,000 cells/plate in P60 TPP plates were exposed to Ag-NPs and the expression level of the target genes were further assayed in a process divided into three steps: i) RNA isolation; ii) RNA reverse transcription; iii) gene expression quantification.

#### 2.11.1. RNA isolation

RNA isolation was performed as described in Section 2.8.

#### 2.11.2. RNA reverse transcription

RNA reverse transcription was performed as previously described (Estevan et al., 2013, 2014). The extracted RNA was reverse transcribed using the Expand Reverse Transcriptase kit and oligo-dT primers (Roche) following the manufacturer's instructions. The reaction mixture (1 μg of RNA and 10 μM oligo-dT primer in a final volume of 10.5 μl of 0.1% (*w/v*) DEPC in water) was heated for 10 min at 65 °C. The following components were then added to the mixture: 1 μl (50 units) of RNA Expand Reverse Transcriptase, 2 μl of 100 mM dithiothreitol, 4 μl of buffer, 2 μl of 10 mM deoxynucleotides, and 0.5 μl of RNase inhibitor. The resulting mixture was incubated at 37 °C for 60 min with a final step of 5 min at 93 °C.

#### 2.11.3. Gene expression quantification

TaqMan® kits (Applied Biosystems) for the following human genes were used: GAPDH (Hs99999905_m1); PGK1 (Hs99999906_m); SPRY 2 (Hs01921749_s1); IL6 (Hs00174131_m1); SPRY 4 (Hs01935412_s1); IL8 (also known as CXCL8) (Hs00174103_m1); JUN B (Hs00357891_s1).

Gene expression was recorded following the supplier's instructions. In short, 10 μl of the TaqMan® Master Mix, 1.0 μl of the TaqMan® assay mix, 2.0 μl of the sample containing 100 ng of cDNA, and 7.0 μl of 0.1% (*w/v*) DEPC in water were treated with the following temperature programme: an initial step at 50 °C for 2 min, 10 min at 95 °C, followed by 40 cycles of 15 s at 95 °C and 60 s at 60 °C.

Changes in gene expression level were estimated relative to the expression of the same gene in control cultures (not exposed to Ag-NPs).

Quantification was performed using the $2^{-\Delta\Delta Ct}$ method (Schmittgen and Livak, 2008). This method uses the expression of a housekeeping gene not affected by the experimental treatments to normalise the expression of the analysed genes.

#### 2.11.4. Selecting housekeeping genes

The selection of the housekeeping genes was performed using the TaqMan™ Array Human Endogenous Controls Plate (Applied Biosystem catalogue no. 4426696), which contains primers for 32 human genes (plated in triplicate), shown to be good candidates to act as human housekeeping genes. T98G cells were exposed to Ag-NPs. Then RNA was isolated as described in Section 2.8 and was reversed transcribed as described above. Approximately 100 ng of cDNA in 5 μl of 0.1% (w/v) DEPC in water were mixed with 5 μl of the TaqMan® Fast Advanced Master Mix (reference catalogue no. 4444556) and transferred to each well to be further subjected to the thermal cycling protocol, as described above.

### 2.12. Interleukin determinations

The concentrations of interleukin (IL) 6 (IL6) and 8 (IL8) in cellular medium were determined by ELISA procedures using the Human IL-6 ELISA Kit (catalogue number KHC0061) and the Human IL-8 ELISA Kit (catalogue number KHC0081), both provided by Invitrogen. Each experimental condition was assayed (for both ILs) during each independent experiment with three biological replicates (3 different wells of the same culture in the same tray). IL6 and IL8 were determined after 24 and 72 h of exposure to Ag-NPs. For both ILs, the 72 h exposure involved three independent experiments, and two for the 24 h exposure. All the experiments were run in the presence of 300 μg/ml of lipopolysaccharides from *Escherichia coli* O55:B5 (MERK, catalogue number L6529) as a positive control.

The T98G human glioblastoma cell cultures seeded on day 0 at 10,000 cells/plate in 96-wells trays were exposed to Ag-NPs. At the end of the exposure time, the supernatant cellular medium was collected and frozen until the time of the IL determination. For such determinations, the provider's instructions were followed. In short, standards or samples (100 μl for IL6 and 50 μl for IL8) were added to the appropriate wells, together with 50 μl Hu IL (6 or 8) Biotin Conjugate solution. Afterwards, the plate was covered, mixed and incubated for 2 (for IL6) or 1.5 (for IL8) h at room temperature. After this incubation, the solution was thoroughly aspirated and wells were washed 4 times with Wash Buffer. Next, 100 μl of Streptavidin-HRP solution were placed in each well, except for the chromogen blanks, and plates were covered with a plate cover and incubated for 30 min at room temperature before thoroughly aspirating the solution from wells and washing wells 4 times with Wash Buffer. The stabilized chromogen (100 μl) was added to each well and incubated for 30 min at room temperature in the dark. The ELISA reaction was ended by adding 100 μl of Stop Solution to each well. Colour was developed for 30 min. Finally, the absorbance at 450 nm was determined and corrected for the non-specific absorption with the absorbance at 570 nm. The IL6 and IL8 concentrations in the supernatant cellular medium were determined by comparing absorbance with the calibrations curves up to 500 pg/ml IL6 and up to 1000 pg/ml IL8 of standards provided with the respective kits.

## 3. Results

### 3.1. Physico-chemical properties of Ag-NPs

The size of particles and their distribution in type I water were assessed by the DLS technique. The mean value for Ag-NPs in a suspension of 1 mg/ml was of 15.96 ± 8.98 nm (Fig. 1A). Fig. 1B displays the recorded mean size and the distribution of sizes and shows how the deviations obtained from the mean are very wide and the distribution of sizes is very broad. These findings suggest the existence of different populations of particle size and lack of colloidal stability in water.

Fig. S2 in Supplementary Material shows the results obtained in the three determinations of the *Z*-potential of the 1 mg/ml suspension of Ag-NPs. The mean value was −35.2 ± 1.52 mV (Fig. 1A). However, as observed in Supplementary Material Fig. S2, peak width is considerable, probably as a result of the different populations of particles present in the suspension, as demonstrated by DLS (Fig. 1B).

The particle size analysis by TEM of Ag-NPs (Fig. 1D) yielded a diameter of 16.56 ± 9.08 nm (Fig. 1A). As shown in Fig. 1C, size dispersion is wide, and was also reported when size was determined by DLS (Fig. 1A).

#### 3.1.1. Stability of Ag-NPs in cell culture medium

Fig. 2 shows the size of Ag-NPs in suspension in type I water and in the RPMI cellular medium supplemented with 10% FBS. No significant variations in populations in size and distribution terms were observed during the analysis time. The sizes with largest proportion of nanoparticles were 10 nm in water and 7.5 nm in cell culture medium for all the tested incubation times. Water suspension exhibited populations of particles whose size equalled or was bigger than 25 nm, which was not observed in cell culture medium.

### 3.2. Effects of Ag-NPs on T98G cell viability

The cytotoxicity of Ag-NPs was assessed by two different well-standardised tests. The percentage of viability of the T98G cultures after the exposure period to 40 μg/ml of Ag-NPs was 95 ± 5 ($n$ = 9) or 100 ± 4 ($n$ = 7) for the MTT and the neutral red uptake test, respectively. It is noteworthy that 40 μg/ml is a concentration that comes quite close to the technically feasible concentration to remain in suspension. The percentage of viability of the T98G cultures after the exposure period to 30 μg/ml of Ag-NPs determined by MTT tests was 92 ± 5 ($n$ = 3). No statistically significant differences were observed between the alterations in viability induced by 30 and 40 μg/ml of Ag-NPs. A decision was made to use 40 μg/ml of Ag-NPs as the default concentration to assess the effects of these NPs on T98G human glioblastoma cells.

### 3.3. Uptake of Ag-NPs in T98G glioblastoma cells

#### 3.3.1. Flow cytometry

T98G cells were firstly exposed to Ag-NPs and afterwards viability and light scattering were analysed by flow cytometry as described in Section 2.6. FSC is proportional to cell size, while SSC is proportional to cell granularity, which should be increased if NPs have been incorporated into cells or remain bound to cytoplasmic membranes.

No significant differences were found between the SSC records obtained in the control cultures and the cultures exposed to Ag-NPs for 24 h and 72 h (Table 1). The cell viability of the cultures was always above 95% (Table 1) in all cases and was, therefore, similar to the viability determined by both the MTT and red neutral uptake tests, as described in Section 3.2.

#### 3.3.2. Microscopy

The cytometry analysis results suggested that Ag-NPs did not come into contact with cells once they had been washed at the end of exposure. We decided to definitively confirm this hypothesis by the TEM and SEM methodologies. To do so, cells were exposed to Ag-NPs and afterwards fixed for electronic microscopy assessment as described in Section 2.7. The results are presented in Fig. 3. No significant differences were detected between the control cultures and the cultures treated with Ag-NPs by SEM and TEM (Fig. 3). It was not possible to detect Ag-NPs by TEM or SEM. Therefore, electronic microscopy confirmed the flow cytometry results, which suggests that Ag-NPs do not come into contact with the T98G cells after washing and fixing the cultures at the end of the exposure period.

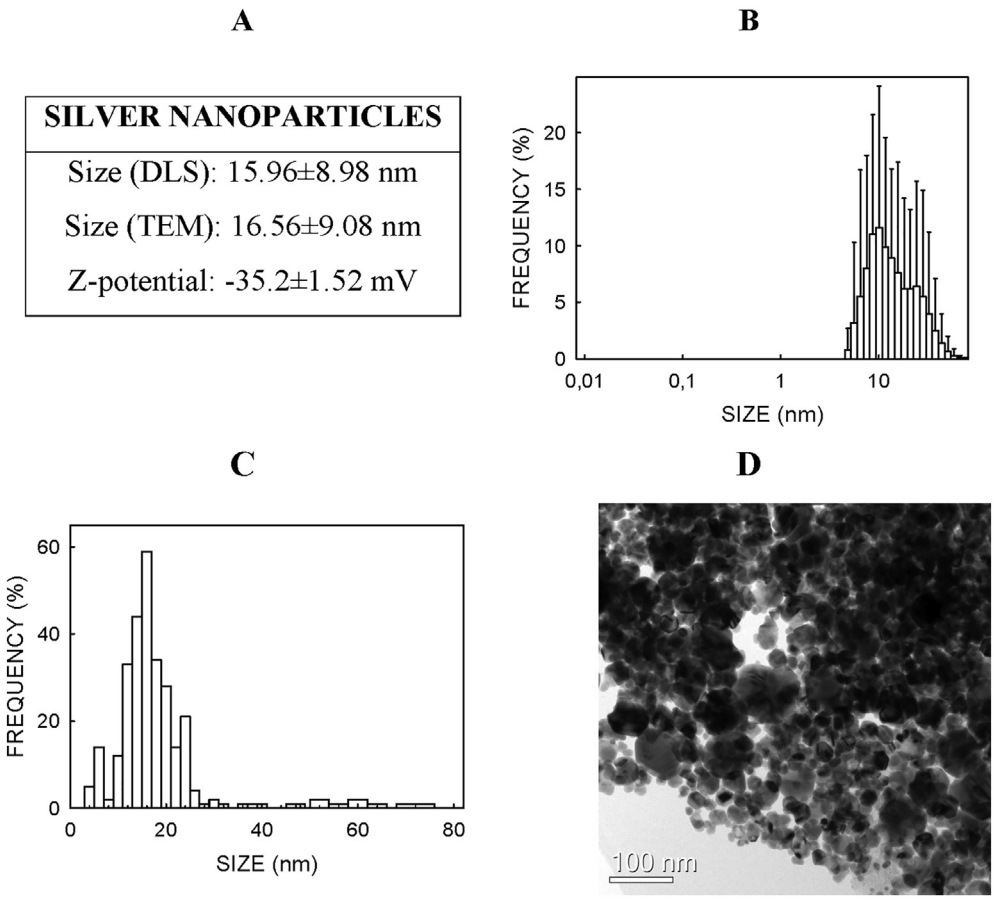


**Fig. 1.** Physico-chemical properties of Ag-NPs. Physical properties (panel A) and distribution of sizes as determined by DLS (panel B) and TEM (panel C). Panel D shows a picture of Ag-NPs under TEM. Fig. S3 in the Supplementary Material displays two other TEM pictures at two different resolutions.

### *3.4. Massively parallel sequencing of RNA of the cells exposed to Ag-NPs*

T98G cells were exposed to Ag-NPs. Afterwards, RNA was isolated as described in Section 2.8 and was sent to MACROGEN Inc. (South Korea) for an RNAseq run on the Illumina NGS platform. Finally, the results were analysed using bioinformatic tools, as described in Section 2.10. Each experimental condition (non-exposed and Ag-NPs-exposed cells) was assayed in triplicate.

#### *3.4.1. RNA quality*

The quality of RNA samples was analysed by Agilent Bioanalyzer 2100 to obtain a RIN for the six samples of 9.7 ± 0.1 (mean ± sd) (range: 9.6–9.8). These samples were sent to South Korea, and MACROGEN further tested the RNA quality of the received material. The RIN value of the samples that arrived to South Korea was 7.7 ± 0.6 (mean ± sd) (range: 7.0–8.3) (see the example in Fig. S4 in the Supplementary Material). Despite loss of RNA quality while transporting all the samples, they went above the RIN threshold of 7.0 and went considered suitable for RNAseq. Fig. S4 in the Supplementary Material shows an example of the electropherograms used to estimate RIN in both our lab and MACROGEN's facilities. In all cases, the three peaks corresponding to ribosomal RNA molecules 5S, 18S and 28S were well defined.

#### *3.4.2. Initial characterisation of the obtained sequences*

Table S1 in the Supplementary Material shows the total number of reads obtained for each sample, the amount of sequences obtained, their GC content, and the proportion of reads with average Phred scores equal to or above 20 (Q20) or 30 (Q30). In all samples, the percentages of reads with Q20 and Q30 values were higher than 98% and 95%, respectively. As expected, the GC content was similar in all the studied samples.

#### *3.4.3. Alignment of the reads to the reference genome*

The reads were aligned to the reference genome using Hisat2 (see Section 2.10) in order to determine the expression level of each gene in the different samples. More than 98% of the reads from each sample aligned to the reference genome (Table 2), with most read pairs aligning concordantly. The rmdup command of samtools was used to assess the frequency of duplicate reads in each sample, which ranged between 26.88% and 33.09%.

#### *3.4.4. Differentially expressed genes*

The statistical analysis was performed with Cuffdiff and allowed the identification of 43 genes expressed at significantly different level in the treated and untreated samples, with a FDR (false discovery rate) of 5% (Table S2 in the Supplementary Material). Of these genes, 13 had higher expression level in the samples treated with Ag-NPs than in the untreated samples, with increases between 1.26-fold ($\log_2$ FC = 0.34) and 8-fold ($\log_2$ FC = 3) (Table S2 in the Supplementary Material). The remaining 30 genes had lower expression level in the treated samples than in the control samples, with reductions ranging between 1.28-fold ($\log_2$ FC = −0.36) and 13.5-fold ($\log_2$ FC = −3.76) (Table S2 in the Supplementary Material). The most over-expressed gene was ENSG00000114857, also known as NKTR, which encodes the natural killer cell triggering receptor (Table S2 in the Supplementary Material). This receptor is a component of a putative tumour-recognition complex involved in the function of NK cells (Uniprot Database accession number P30414). The most repressed gene was ENSG00000120738, also known as EGR1, which encodes the early growth response 1

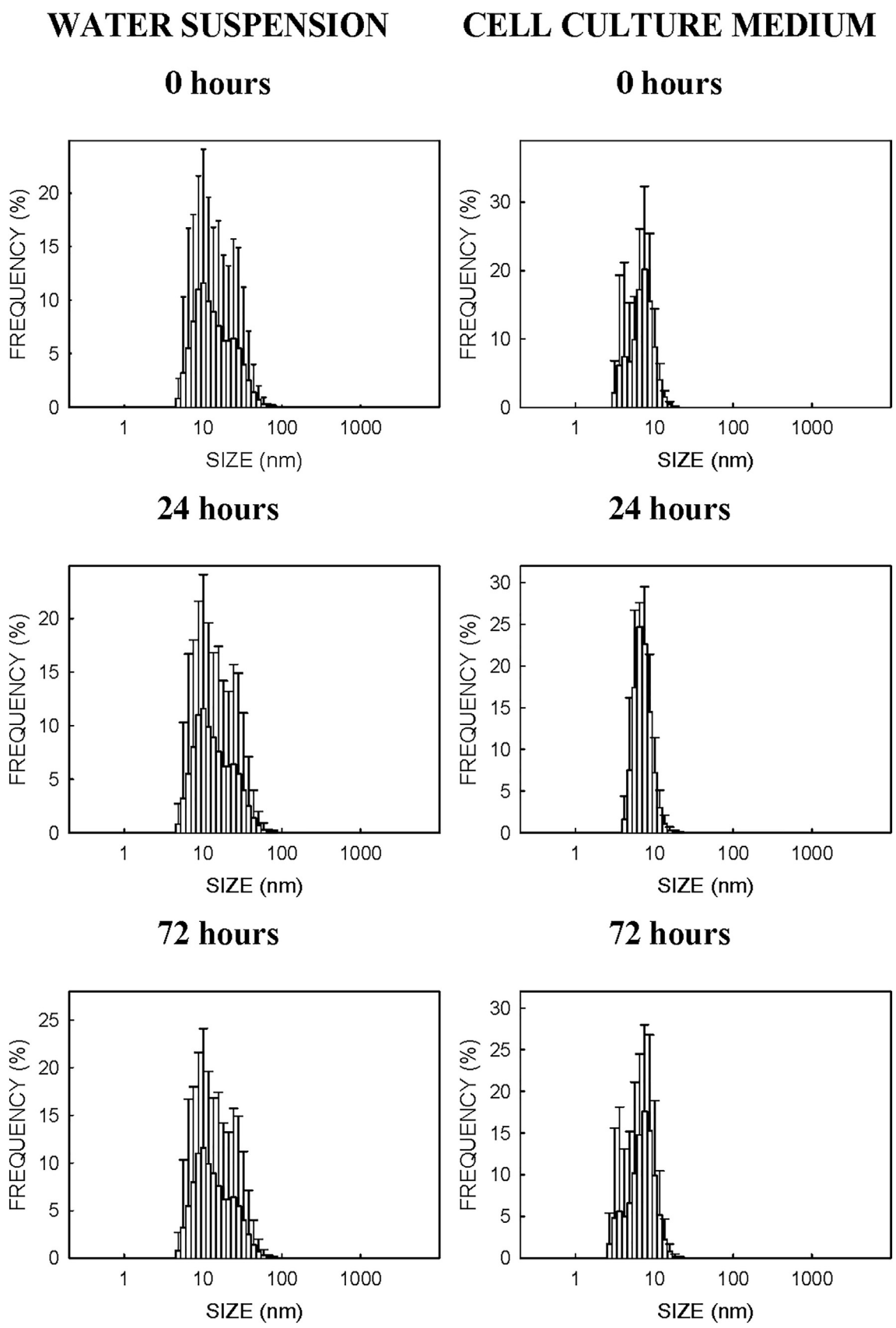


**Fig. 2.** Analysis of the size and distribution of Ag-NPs in water (left panels) and cell culture medium (right panels). Size was determined by DLS. Cell culture medium were RPMI cellular medium supplemented with 10% FBS.

**Table 1**
Mean side scatter (SSC) and viability of the cell cultures exposed to 40 μg/ml of Ag-NPs. Cells were exposed to NPs as described in Section 2.4 and were then treated as described in Section 2.6 for flow cytometry. Two biological replicates were used for each experiment. Here we see the individual records of the biological replicates and their respective means (in brackets). Viability was determined using propidium iodide only in the second experiment. Ratios were estimated with the means as SSC sample/SSC control.

| | Experiment 1 (72 h) | | Experiment 2 (24 h) | | | Experiment 2 (72 h) | | |
|---|---|---|---|---|---|---|---|---|
| | SSC | Ratio | SSC | Ratio | Viability (%) | SSC | Ratio | Viability (%) |
| Control | 1168 | | 1038 | | 98 | 816 | | 98 |
| | 1186 (1177) | | 979 (1009) | | 98 | 680 (748) | | 96 |
| | | 1.00 | | 1.00 | (98) | | 1.00 | (97) |
| Ag-NPs | 1238 | | 1111 | | 97 | 1014 | | 98 |
| | 1286 (1262) | | 1131 (1121) | | 98 | 1036 (1025) | | 97 |
| | | 1.07 | | 1.11 | (97.5) | | 1.37 | (97.5) |

protein (Table S2 in the Supplementary Material). This transcription factor plays a role in the recognition and DNA binding in the promoter region of target genes, regulation of cell survival, proliferation and cell death and activation of p53/TP53 and TGFB1 with the subsequent prevention of tumour formation (Uniprot Database accession number P18146).

In order to display these results, a heat map was prepared with the normalised expression values for each sample (Fig. S5 in the Supplementary Material). The dendrograms were obtained by applying a clustering algorithm to samples and differentially expressed genes. As expected, both the treated and untreated samples defined clearly distinct groups.

### 3.4.5. Annotation of differentially expressed genes

To better understand the functions affected by the treatment with Ag-NPs, the GO terms associated with the set of differentially expressed genes were analysed with the GO Consortium tool. An enrichment analysis based on Fisher's exact tests was performed to identify terms overrepresented among the set of differentially expressed genes, as implemented in the PANTHER Classification System tool. The FDR was used to control excess false positives. As a control set, we used the 11,869 genes expressed in the studied samples (Table S3 in the Supplementary Material), which were chosen instead of the default set offered by the tool. Of the 11,869 genes expressed in T98G cells, 11,260 were assigned at least one GO term, while 40 of the 43 genes with significantly different expression level (Table S2 in Supplementary Material) had at least one associated GO term.

The results for the "*biological process*" sub-ontology are presented on Table 3. In this sub-ontology, several terms related to inflammation were highly enriched among the set of genes differentially expressed as

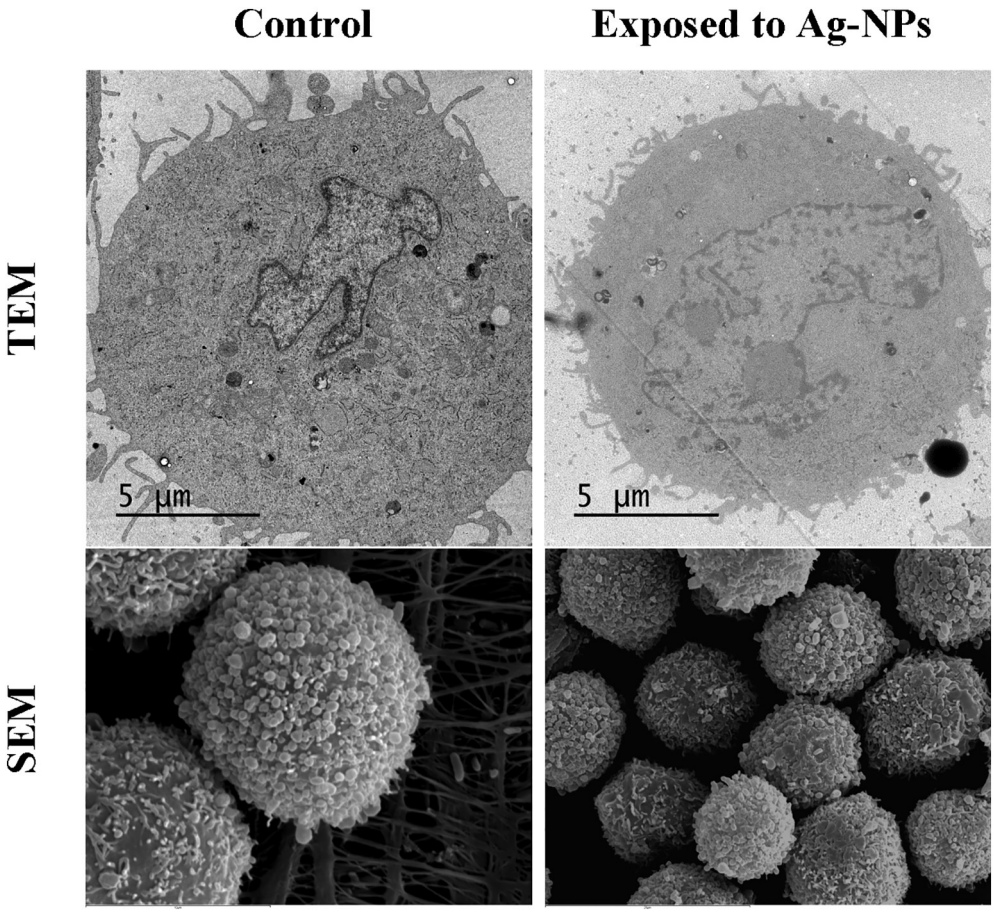


**Fig. 3.** T98G human glioblastoma cells visualized by TEM and SEM. A second independent culture yielded similar results.

**Table 2**
Alignment of sequences to the reference genome.

| | Control | | | Ag NPs | | |
|---|---|---|---|---|---|---|
| Readings | 1 | 2 | 3 | 1 | 2 | 3 |
| Initial | 31,016,624 | 30,419,346 | 32,022,288 | 37,267,912 | 34,912,942 | 31,894,022 |
| Filtered | 26,681,128 | 26,192,232 | 26,451,976 | 32,773,468 | 31,186,266 | 25,943,390 |
| Aligned (%) | 26,342,795 (98.73) | 25,793,274 (98.48) | 26,083,336 (98.61) | 32,379,051 (98.80) | 30,810,044 (98.79) | 25,661,862 (98.91) |
| Duplicated (%) | 28.12 | 28.09 | 26.88 | 33.09 | 28.61 | 27.98 |

a consequence of exposure to Ag-NPs. The term "*positive regulation of the acute inflammatory response*" (GO:0002675) exhibited the highest enrichment factor (80.4) among the 31 enriched biological processes (Table 3). Other enriched terms were "*response to the interleukin-6*" (GO:0070741), "*cellular response to the cytokine stimulus*" (GO:0071345) and "*response to lipopolysaccharide*" (GO:0032496) (a well-known inductor of neuro-inflammation), with enrichment factors of 36.7, 4.6 and 8.7, respectively (Table 3).

Another altered biological process with a potential impact in glia performance was the "*negative regulation of the fibroblast growth factor (FGF) receptor signalling pathways*" (GO:0040037) (the biological process with the second highest enrichment factor), the "*regulation of astrocyte differentiation*" (GO:0048710) and the "*response to wounding*" (GO:0009611), with enrichment factors of 76.7, 46.9 and 5.9, respectively (Table 3).

The expressions of the genes related to the signalling pathways through serine/threonine protein kinases seemed to also be severely affected by exposure to Ag-NPs. This outcome was suggested by the fact that the genes involved in the biological processes of "*inactivation of MAPK activity*" (GO:0000188), the "*negative regulation of Extracellular-signal Regulated Kinase 1 (ERK1) and 2 (ERK2) cascade*" (GO:0070373) and "*positive regulations of ERK1 and 2 ERK2 cascade*" (GO:0070374) and the "p*ositive regulation of protein kinase B signalling*" (GO:0051897) were enriched with factors ranging between 15.1 and 40.2 (Table 4). Moreover, the genes involved in "*MAP kinase tyrosine/serine/threonine phosphatase activity*" and "*MAP kinase phosphatase activity*" (GO:0033549) of the molecular function sub-ontology were also highly overrepresented (enrichment factors of 84.4 and 76.7, respectively) among these differentially expressed genes after exposure to Ag-NPs (Table 4).

### 3.4.6. Altered molecular pathways

The altered molecular pathways were also analysed using PANTHER and reported 12 altered pathways (Table 5). Four of these pathways were represented by a single differentially expressed gene (p38 MAPK pathway, angiotensin II-stimulated signalling through G proteins and the beta-arrestin pathway, Notch signalling pathway and the cadherin signalling pathway). Four additional pathways were represented by two differentially expressed genes (CCKR signalling map, the TGF-beta signalling pathway, the interleukin signalling pathway and the FGF signalling pathway). Finally, the gonadotropin releasing hormone receptor pathway, oxidative stress response, inflammation mediated by chemokine and the cytokine signalling pathway, and the Epidermal Growth Factor (EGF) receptor signalling pathway were the pathways

**Table 3**
The biological process ontology terms overrepresented in the differentially expressed genes in the T98G human glioblastoma exposed for 72 h to 40 μg/ml of Ag-NPs. Only the results for FDR p < 0.05 are displayed. DEG = Differentially Expressed Genes; EF = Enrichment factor; FDR = False Discovery Rate.

| Biological process sub-ontology (GO term) | Genes in reference list | Genes among DEG | Expected among DEG | EF | P value | FDR |
|---|---|---|---|---|---|---|
| Positive regulation of acute inflammatory response (GO:0002675) | 7 | 2 | 0.02 | 80.4 | 4.33E-04 | 4.09E-02 |
| Negative regulation of FGF receptor signalling pathway (GO:0040037) | 11 | 3 | 0.04 | 76.7 | 1.46E-05 | 6.41E-03 |
| Peptidyl-threonine dephosphorylation (GO: 0035970) | 15 | 3 | 0.05 | 56.3 | 3.24E-05 | 8.13E-03 |
| Labyrinthine layer blood vessel development (GO:0060716) | 16 | 3 | 0.06 | 52.8 | 3.83E-05 | 8.85E-03 |
| Regulation of astrocyte differentiation (GO:0048710) | 18 | 3 | 0.06 | 46.9 | 5.24E-05 | 1.01E-02 |
| Inactivation of MAPK activity (GO:0000188) | 21 | 3 | 0.07 | 40.2 | 7.91E-05 | 1.36E-02 |
| Response to interleukin-6 (GO:0070741) | 23 | 3 | 0.08 | 36.7 | 1.01E-04 | 1.60E-02 |
| Positive regulation of tyrosine phosphorylation of STAT protein (GO:0042509) | 25 | 3 | 0.09 | 33.8 | 1.27E-04 | 1.80E-02 |
| Positive regulation of osteoblast differentiation (GO:0045669) | 39 | 4 | 0.14 | 28.9 | 1.51E-05 | 6.06E-03 |
| Regulation of epidermal cell differentiation (GO:0045604) | 32 | 3 | 0.11 | 26.4 | 2.49E-04 | 2.97E-02 |
| Negative regulation of ERK1 and ERK2 cascade (GO:0070373) | 50 | 4 | 0.18 | 22.5 | 3.75E-05 | 8.81E-03 |
| Positive regulation of T cell proliferation (GO:0042102) | 39 | 3 | 0.14 | 21.6 | 4.29E-04 | 4.11E-02 |
| Reactive oxygen species metabolic process (GO:0072593) | 58 | 4 | 0.21 | 19.4 | 6.49E-05 | 1.20E-02 |
| Positive regulation of protein kinase B signalling (GO:0051897) | 89 | 5 | 0.32 | 15.8 | 1.87E-05 | 6.14E-03 |
| Peptidyl-tyrosine dephosphorylation (GO:0035335) | 73 | 4 | 0.26 | 15.4 | 1.51E-04 | 2.09E-02 |
| Positive regulation of ERK1 and ERK2 cascade (GO:0070374) | 93 | 5 | 0.33 | 15.1 | 2.30E-05 | 6.87E-03 |
| Regulation of fat cell differentiation (GO:0045598) | 78 | 4 | 0.28 | 14.4 | 1.93E-04 | 2.45E-02 |
| Response to corticosteroid (GO:0031960) | 83 | 4 | 0.29 | 13.6 | 2.43E-04 | 2.92E-02 |
| Lung development (GO:0030324) | 109 | 5 | 0.39 | 12.9 | 4.76E-05 | 9.71E-03 |
| Response to lipopolysaccharide (GO:0032496) | 161 | 5 | 0.57 | 8.7 | 2.80E-04 | 3.11E-02 |
| Regulation of epithelial cell proliferation (GO:0050678) | 197 | 6 | 0.70 | 8.6 | 7.22E-05 | 1.29E-02 |
| Blood vessel morphogenesis (GO:0048514) | 254 | 7 | 0.90 | 7.8 | 3.15E-05 | 8.22E-03 |
| Cellular response to growth factor stimulus (GO:0071363) | 324 | 8 | 1.15 | 7.0 | 1.73E-05 | 6.25E-03 |
| Regulation of system process (GO:0044057) | 254 | 6 | 0.90 | 6.7 | 2.79E-04 | 3.15E-02 |
| Response to wounding (GO:0009611) | 332 | 7 | 1.18 | 5.9 | 1.64E-04 | 2.15E-02 |
| Positive regulation of protein kinase activity (GO:0045860) | 347 | 7 | 1.23 | 5.7 | 2.14E-04 | 2.64E-02 |
| Nervous system process (GO:0050877) | 368 | 7 | 1.31 | 5.4 | 3.04E-4 | 3.27E-2 |
| Cellular response to cytokine stimulus (GO:0071345) | 617 | 10 | 2.19 | 4.6 | 4.81E-05 | 9.67E-03 |
| Negative regulation of cell death (GO:0060548) | 639 | 9 | 2.27 | 4.0 | 3.50E-04 | 3.52E-02 |
| Tissue development (GO:0009888) | 906 | 12 | 3.22 | 3.7 | 5.09E-05 | 1.01E-02 |
| Regulation of apoptotic process (GO:0042981) | 1006 | 13 | 3.58 | 3.6 | 2.89E-05 | 7.68E-03 |

**Table 4**
The molecular function ontology terms overrepresented in the differentially expressed genes in the T98G human glioblastoma exposed for 72 h to 40 μg/ml of Ag-NPs. Only the results for FDR p < 0.05 are displayed. DEG = Differentially Expressed Genes; EF = Enrichment factor; FDR = False Discovery Rate.

| Molecular function sub-ontology (GO term) | Genes in reference list | Genes among DEG | Expected among DEG | EF | P value | FDR |
|---|---|---|---|---|---|---|
| MAP kinase tyrosine/serine/threonine phosphatase activity (GO:0017017) | 10 | 3 | 0.04 | 84.4 | 1.15E-05 | 4.56E-02 |
| MAP kinase phosphatase activity (GO:0033549) | 11 | 3 | 0.04 | 76.7 | 1.46E-05 | 2.90E-02 |

with the most genes with an altered expression (three for all these pathways) (Table 5).

### 3.5. Validation of massively parallel sequencing by PCR

Five different genes were selected to validate the RNAseq results, namely: transcription factor jun-B (JUN B) (with an altered expression in three different molecular pathways after exposure to Ag-NPs (Table 5)); interleukin-6 (IL6) (with an altered expression in two different molecular pathways after exposure to Ag-NPs (Table 5)); interleukin-8 (IL8) (with no altered expression in the pathways outlined in Table 5 but with a down-regulation of 53% found in the RNAseq experiment (Table S2 in the Supplementary Material); protein sprouty homolog 2 (SPRY 2) and protein sprouty homolog 4 (SPRY 4) (both with an altered expression in two different molecular pathways after exposure to Ag-NPs (Table 5)).

#### 3.5.1. Selecting housekeeping genes

We tested the effect of Ag-NPs on the expression of 24 different human genes that are typically used as housekeeping genes (see Section 2.11). The results are shown on Table S4 in the Supplementary Material. Ag-NPs had no statistically significant effect on the expression of 22 of the 24 assessed genes, while the number of thermal cycles needed to reach the fluorescence threshold in the PCR was statistically increased for 18S rRNA and dropped for CDKN1B (Table S4 in the Supplementary Material). The housekeeping genes GAPDH (glyceraldehyde 3-phosphate dehydrogenase) and PGK1 (phosphoglycerate kinase 1) were selected, as their expression level were not altered by Ag-NPs and they are often used for this purpose in the scientific literature.

#### 3.5.2. Expressions of the selected genes

The expression level of the above-cited genes was assayed with two different housekeeping genes and in two independent experiments. The T98G human glioblastoma cells were exposed to Ag-NPs using the same conditions as in the RNAseq experiments (40 μg/ml for 72 h). RNA was then isolated as described in Section 2.8 and the expression level of each gene was tested by RT-PCR, as described in Section 2.11. Three different plates per experimental condition were used in each independent experiment.

Ag-NPs brought about a statistically significant reduction in the IL6 expression of around 55% in the samples assayed by both RNAseq and RT-PCR (Table 6), while these NPs lowered the IL8 expression by around 35%, although the statistical significance was reached only with GAPDH as housekeeping gene, but not with PGK1 or in the RNAseq experiment (Table 6). Ag-NPs caused a statistically significant reduction in the expression level of the JUN B gene (Table 6). The extent of this reduction was around 50–60% when determined by both RT-PCR and RNAseq (Table 6). Ag-NPs also caused statistically significant reductions in the expression level of the SPRY 2 and SPRY 4 genes, but the reduction was more marked for SPR 4 (about 40–60%) than for SPRY 2 (approx. 20%) (Table 6). In general, the effects of Ag-NPs matched well the changes in the expression of these genes assessed by both RNAseq and RT-PCR (Table 6). The results of the two independent RT-PCR experiments were reproducible, and no differences were detected when the effects were assessed using GAPDH or PGK1 as housekeeping genes (Table 6).

**Table 5**
Molecular pathways altered in T98G human glioblastoma exposed during 72 h to 40 μg/ml of Ag-NPs.

| Pathway | Genes involved | $Log_2$ fold change |
|---|---|---|
| CCKR signalling map | Radiation-inducible immediate-early gene IEX-1 | −0.75 |
| | Early growth response protein 1 | −3.76 |
| Gonadotropin releasing hormone receptor pathway | Early growth response protein 1 | −3.76 |
| | Epidermal growth factor receptor | 0.34 |
| | Transcription factor jun-B | −1.06 |
| p38 MAPK pathway | Dual specificity protein phosphatase 10 | −0.74 |
| Angiotensin II-stimulated signalling through G proteins and beta-arrestin | Early growth response protein 1 | −3.76 |
| TGF-beta signalling pathway | Transcription factor jun-B | −1.06 |
| | Growth/differentiation factor 15 | −0.81 |
| Oxidative stress response | Dual specificity protein phosphatase 10 | −0.74 |
| | Dual specificity protein phosphatase 5 | −0.64 |
| | Dual specificity protein phosphatase 4 | −0.86 |
| Notch signalling pathway | Transcription factor HES-1 | −1.40 |
| Interleukin signalling pathway | Interleukin-6 | −0.90 |
| | Interleukin-6 receptor subunit beta | 0.65 |
| Inflammation mediated by chemokine and cytokine signalling pathway | Transcription factor jun-B | −1.06 |
| | Interleukin-6 | −0.90 |
| | C−C motif chemokine 2 | −1.09 |
| FGF signalling pathway | Protein sprouty homolog 4 | −1.67 |
| | Protein sprouty homolog 2 | −0.69 |
| EGF receptor signalling pathway | Epidermal growth factor receptor | 0.34 |
| | Protein sprouty homolog 4 | −1.67 |
| | Protein sprouty homolog 2 | −0.69 |
| Cadherin signalling pathway | Epidermal growth factor receptor | −3.76 |

**Table 6**
Effects of Ag-NPs on the expressions of different genes. T98G human glioblastoma cells were exposed to Ag-NPs. Then RNA was isolated as described in Section 2.8, and was retrotranscribed and quantified by RT-PCR as described in Section 2.11 using GAPDH and PGK1 as housekeeping genes. The RNAseq data were taken from the respective $\log_2$ (fold change) shown in Table S2 in the Supplementary Material. * = Statistically different from the control for $p < 0.05$. ** = Statistically different from the control for $p < 0.01$.

| | | Relative expression PCR experiment 1 | | Relative expression PCR experiment 2 | |
|---|---|---|---|---|---|
| Gene | RNAseq | GAPDH | PGK1 | GAPDH | PGK1 |
| IL6 | 0.53* | 0.57 ± 0.09** | 0.58 ± 0.11* | 0.54 ± 0.08* | 0.55 ± 0.12* |
| IL8 | 0.67 | 0.66 ± 0.09** | 0.67 ± 0.03 | 0.62 ± 0.02* | 0.65 ± 0.22 |
| JUN B | 0.48* | 0.41 ± 0.06** | 0.42 ± 0.06** | 0.44 ± 0.07** | 0.44 ± 0.19 |
| SPRY 2 | 0.62* | 0.81 ± 0.10** | 0.83 ± 0.15* | 0.73 ± 0.09 | 0.78 ± 0.33 |
| SPRY 4 | 0.31* | 0.42 ± 0.03** | 0.43 ± 0.05** | 0.35 ± 0.07** | 0.38 ± 0.20** |

#### 3.5.3. Effect of concentration on the alterations to gene expressions induced by Ag-NPs

T98G human glioblastoma cells were exposed to three different concentrations (40, 4 and 0.4 μg/ml) of Ag-NPs for 72 h. After exposure ended, RNA was isolated as described in Section 2.8 and the expression of each gene was determined by RT-PCR using GAPDH as housekeeping gene as described in Section 2.11. Each experimental condition was assayed in three different biological replicates. The results are shown in Fig. 4.

The highest dose of Ag-NPs caused no significant effects on the expression level of the SPRY 2, IL6 and IL8 genes (Fig. 4B, C and D). The effects of Ag-NPs on the expression of gene JUN B were statistically significant, but only at 40 μg/ml (Fig. 4E). Ag-NPs caused a dose-dependent statistically significant decrease in the expression of gene SPRY 4, and 4 μg/ml was the lowest dose to produce an observable effect (Fig. 4A). In all cases, the relative expression at 40 μg/ml was comparable to the relative expression described in Table 6, except for IL8, whose higher SD might mask the results and the statistical significance reported on Table 6. Something similar (albeit to a lesser extent) could have occurred for the highest concentration of both SPRY 2 and IL6, and lack of statistical significance (detected in Table 6) could have been caused by a relatively high SD.

### 3.6. Effect of Ag-NPs on the secretion of IL6 and IL8

The expression of genes IL6 and IL8 was moderately down regulated after 72 h of exposure to Ag-NPs (Table 6). A check was made to see if this down-regulation was reflected phenotypically by determining the amounts of IL6 and IL8 secreted to supernatant cellular medium by T98G cells after 24 h and 72 h of exposure to 40 μg/ml of Ag-NPs. The differences in IL6 and IL8 secreted after both the 24- and 72 h exposures between the control cultures and cultures exposed to both Ag-NPs and lipopolysaccharides from *Escherichia coli* O55:B5 (positive control) were always statistically significant (Table 7).

The amount of IL8 secreted after exposure to the positive control (lipopolysaccharides from *Escherichia coli* O55:B5) was always larger than the IL6 secreted after the comparable exposure (Table 7). The secretion of both IL6 and IL8 after exposure to Ag-NPs was always statistically lower than controls. Fig. 5 shows the distribution of all the individual determinations, with a tendency of IL6 and IL8 to yield lower values than the respective controls with a very small area of overlapping values among the lower control values with higher values for the treated samples. Fig. 5 shows no overlapping between the records of the control cultures and the cultures exposed to the positive control because the latter was always higher.

## 4. Discussion

This work has studied the effects of Ag-NPs on T98G human glioblastoma cells using a wide array of methodologies, including RNAseq, RT-PCR, microscopy and flow cytometry. The physico-chemical characterisation of Ag-NPs reported that the mean size of NPs in cell culture medium was slightly smaller than in water suspension (Fig. 2). The reduction in the particle size in the presence of cell culture medium could be attributed to the presence of the proteins that help dispersion if the NPs in the suspension thus lowered the number of aggregates. This phenomenon has already been reported by other authors (Schulze et al., 2008; Zhang et al., 2008; Powers et al., 2007). At any rate, it was noteworthy that the condition of NP was not loss during the window of exposure (0–72 h) in our experiments because the mean size was always clearly below 100 nm (Fig. 2) and, therefore, no aggregates were formed that could impair the condition of NPs.

T98G cells are a polyploid variant of T98 cells, T98G cells are like normal cells in that they become arrested in G1 phase under stationary phase conditions, yet they also exhibit the transformed immortality (Stein, 1979). Our lab, in an attempt to explore the possible functional differences between the T98G cells and the human glial cells, has performed a differential expression analysis using the software packages cited in Section 2.10 plus ballgown (Pertea et al., 2016). For the differential expression analysis, we compared the 467 human glial cells transcriptomes obtained from SRA database under the accession number SRP057196 with the three transcriptomes of T98G cells obtained in our control plates of the RNAseq experiment. We found 4875 of 24,628 genes differentially expressed. In this set of 4875 differentially expressed genes an analysis of over-representation was made, showing no over or under-represented pathways as compared with the total expressed genes. However taken into account only the under-expressed genes ($n = 966$) the ionotropic glutamate receptor pathway and the β-1 adrenergic receptor signalling pathway were over-represented (FDR $< 0.05$). All these data allow conclude that T98G cells has only minimum cellular pathways over- or under-represented in comparison with primary human glial cells and therefore, no drastic differences in their capacity of response against xenobiotic can be expected. Indeed, T98G cells have already been used by other authors for testing the effects of xenobiotic on glial cells (Panossian et al., 2019).

### 4.1. Cytotoxicity

Human T98 glioblastoma cells were relatively resistant to the cytotoxicity induced by Ag-NPs. Indeed, the exposure to 40 μg/ml Ag-NPs for 72 h reduced cell viability by only 5%. This finding strongly contrasts with BALB/c 3 T3 fibroblasts, U937 monocytes and NR8383 macrophages, whose viability was reduced by 50% after a 24 h exposure to 3.1, 6.7 and 9.8 μg/ml, respectively, of polyvinylpyrrolidone-coated Ag-NPs whose size was 20 ± 7 nm (Mannerström et al., 2016).

Other oxide metallic NPs, such as magnetite ($Fe_3O_4$), were more cytotoxic in human brain cell cultures. Indeed magnetite induced significant cytotoxicity (through mitochondria impairment) in D384 astrocytes after 48 h of exposure, starting with 1 μg/ml (Coccini et al., 2017). However, SH-SY5Y human neuroblastoma was less susceptible to magnetite than D384 astrocytes, as cytotoxicity occurred after 48 h with only 35–45% mortality at the 10–100 μg/ml concentrations

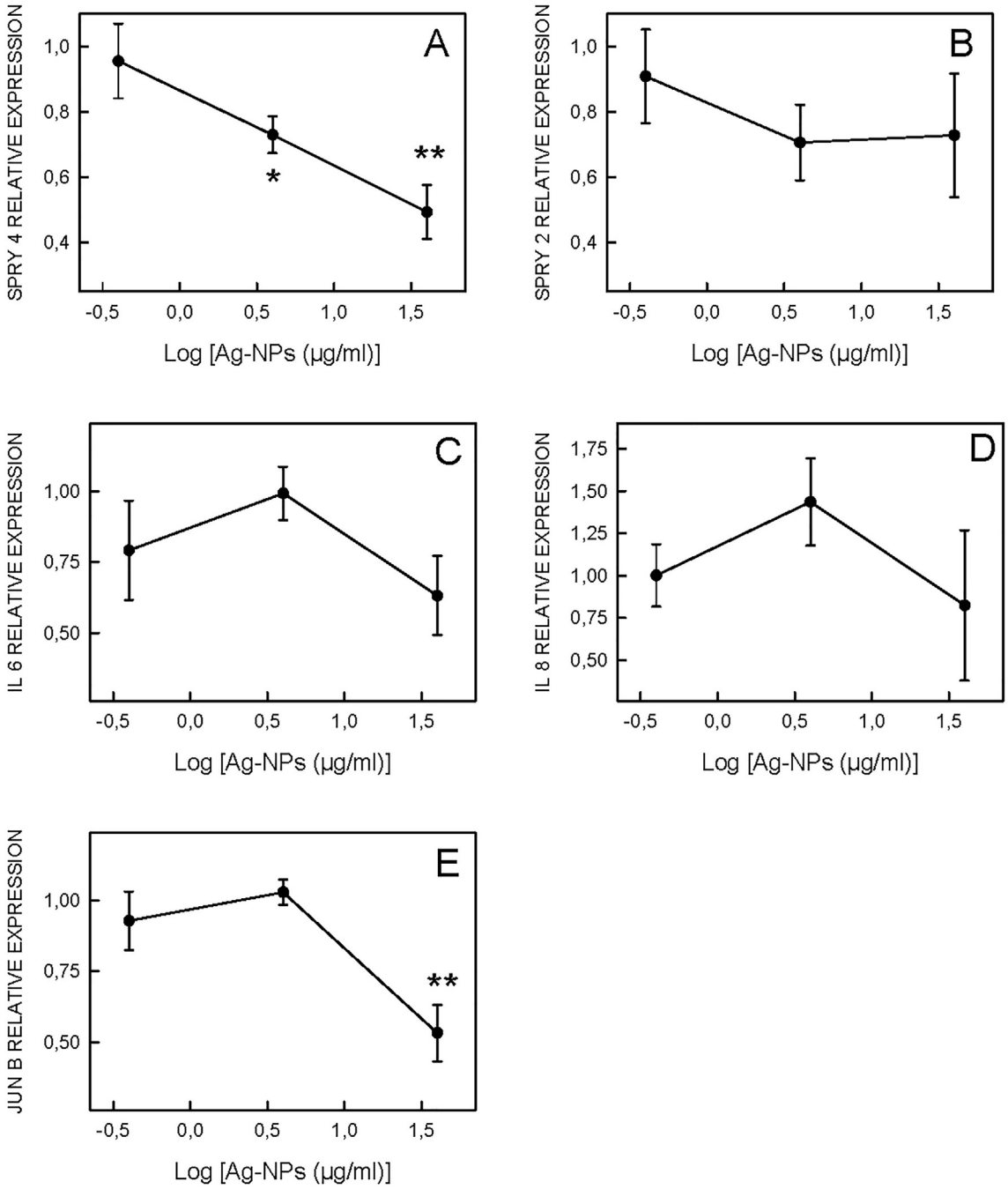


**Fig. 4.** Effect of the concentration on the alterations of the gene expressions induced by Ag-NPs. The means ± SD of three biological replicates are displayed. * = Statistically different from the control for $p < 0.05$. ** = Statistically different from the control for $p < 0.01$.

(Coccini et al., 2017).

### 4.2. NP uptake

It is known that metallic NPs such as $TiO_2$ can be taken up by cells such as ARPE-19 (cultured human-derived retinal pigment epithelial cells) (Zucker et al., 2010). The uptake of Ag-NPs has been proven in certain lines; *e.g.*, it has been demonstrated that polyvinylpyrrolidone-coated Ag-NPs at µM concentrations for up to 24 h accumulate in time-, temperature- and concentration-dependent manners in astrocyte-rich primary cultures by an endocytosis mechanism with no significant cytotoxicity (Luther et al., 2011). However, microscopy and scattering flow cytometry demonstrated that Ag-NPs did not accumulate in T98G human glioblastoma after 72 h of exposure at concentrations that came close to the solubility limit (Table 1, Fig. 3). We are unable to explain this difference, which might be due to several factors like size, shape or coating of the NPs.

### 4.3. Altered biological process and molecular pathways: neuro-inflammation

The exposure of T98 human glioblastoma cells to 40 µg/ml of Ag-NPs for 72 h barely reduced cell viability, but significantly altered the expression of 43 genes, the majority of which were down-regulated (Table S2 in the Supplementary Material).

The assessment of genes with a statistically altered expression with the GO terms indicated an association with several biological processes that address neuro-inflammation, such as the *"positive regulation of acute*

**Table 7**
Effect of Ag-NPs on the secretion of IL6 and IL8 by T98G cells. T98G cells were exposed to 40 μg/ml of Ag-NPs for 24 or 72 h. Afterwards IL determinations were made following ELISA procedures, as described in Section 2.12. Each experimental condition within each independent experiment was performed with three different wells. The contents of IL in the control (unexposed) wells was considered 100%. The treatment done with 300 μg/ml of lipopolysaccharides from *Escherichia coli* O55:B5Y was considered the positive control. The control cultures secreted after the 72 h exposure 1810, 1864 and 1898 pg IL6/ml in experiments 1, 2 and 3, respectively. The control cultures secreted after the 72 h exposure 618, 718 and 644 pg IL8/ml in experiments 1, 2 and 3, respectively. The control cultures secreted after the 24 h exposure 572 and 724 pg IL6/ml in experiments 1 and 2, respectively. The control cultures secreted after the 24 h exposure 282 and 370 pg IL8/ml in experiments 1 and 2, respectively. * = Statistically different from the control for at least $p < 0.05$. Fig. 5 shows the distributions of all the individual determinations expressed as pg/ml.

| | | IL6 (%) | IL8 (%) |
|---|---|---|---|
| *72 h exposure* | | | |
| Experiment 1 | Ag-NPs | 86* | 76* |
| | Positive control | 114* | 217* |
| Experiment 2 | Ag-NPs | 90* | 76* |
| | Positive control | 113* | 223* |
| Experiment 3 | Ag-NPs | 91* | 88* |
| | Positive control | 114* | 230* |
| *24 h exposure* | | | |
| Experiment 1 | Ag-NPs | 79* | 80* |
| | Positive control | 176* | 315* |
| Experiment 2 | Ag-NPs | 84* | 71* |
| | Positive control | 167* | 228* |

*inflammatory response*" (GO:0002675) (enrichment factor 80), "*response to interleukin-6*" (GO:0070741) (enrichment factor 37) and "*cellular response to cytokine stimulus*" (GO:0071345) (enrichment factor 7) (Table 3). Moreover, those genes with an altered expression were also addressed for "*inflammation mediated via the chemokine and cytokine signalling pathway*" and the "*interleukin signalling pathway*" due to the down-regulation in the expression of transcription factor jun-B (52%), interleukin-6 (47%) and chemokine receptor C−C motif chemokine 2 (53%) (Table 5). The reduction in IL6 expression reduces symptoms in autoimmune diseases, however, increased bacterial infections may ensue (Rose-John, 2018). IL6 is one of the first actors that contributes to defence through the stimulation of acute phase responses (Tanaka et al., 2014) (the biological process with the highest enrichment factor among the genes with a significantly altered expression) and IL8 is also a pro-inflammatory IL as well. Therefore, the reduction in the expression level of the genes coding for IL6 and IL8 (Table 6) as well as the reduction in IL6 and IL8 secretion (Table 7; Fig. 5) might reduce the central nervous system's defence capability against other stressing agents, such as bacteria or virus, through impairment of inflammation mechanisms. Although on the other hand, the reduction in the IL6 and IL8 secretion (Table 7; Fig. 5) might be also consistent with the anti-inflammatory effects reported in immortalized embryonic mouse microglia N9 cell line (Gonzalez-Carter et al., 2017).

The reduction in the inflammatory response caused by Ag-NPs as a consequence of the reduction in IL6 and IL8 seemed to be an opposite effect caused by other NPs in glia, such as $SiO_2$-NPs, which caused the release of pro-inflammatory cytokines to the primary culture of rat microglia and the inflammation of the blood brain barrier in rats (Migliore et al., 2015). Our results also contrast with the overexpression of the genes involved in immune and inflammatory processes in the offspring of mice exposed *in utero* to Ag-NPs (Amiri et al., 2018). In this case, however, the inflammatory process was not specific of the nervous system, as reported herein due to the used cellular model.

### 4.4. Altered biological process and molecular pathways: fibroblast growth factor

The "*negative regulation of the FGF receptor signalling pathway*" (GO:0040037) was the biological process with the second highest enrichment factor (77) among the set of genes with significantly altered expression level after exposure to Ag-NPs (Table 3). This was supported by the alteration of the "*FGF signalling pathway*", as reported in Table 5, due to the down-regulation of genes protein sprouty homolog 4 (69%) and protein sprouty homolog 2 (38%), which are involved in the "*EGF receptor-transduced MAPK signalling pathway*" (this pathway was also altered; see Table 5) and in the antagonism of the FGF pathways, respectively (Uniprot Database accession numbers O43597 and Q9C004). The FGF receptor is coupled *via* an intracellular kinase domain by the phosphorylation of specific tyrosine residues to, among others, RAS-MAPK and signal transducer and activator of transcription (STAT) pathways (Ornitz and Itoh, 2015). Table 3 shows how biological process "*peptidyl-tyrosine dephosphorylation*" (GO:0035335) (enrichment factor 15) and the "*positive regulation of tyrosine phosphorylation of the STAT protein*" (GO:0042509) (enrichment factor 34) are over-represented among the pool of genes whose expression were altered after exposure to Ag-NPs. Thus, Table 3 provides several entries that, in general, are strongly consistent with an alteration to the FGF receptor-signalling pathway.

FGFs are a group of polypeptides that act in early embryonic development stages and during organogenesis. FGFs also play a role in adult tissues where they mediate metabolic, repair and regeneration functions, often by reactivating developmental signalling pathways (Ornitz and Itoh, 2015). FGFs are distributed in many adult tissues, but there is a glial-specific FGF (FGF 9) that is required for both neuronal migration and the translocation of astroglial cells (Ornitz and Itoh, 2015). It is noteworthy that T98G is a multiform glioblastoma; that is, it includes astrocytes. Therefore, their role might be altered as consequence of the deregulation of the FGF signalling pathway derived from exposure to Ag-NPs. FGF9 might also play a role in glial cell growth and differentiation, gliosis, differentiation and survival of

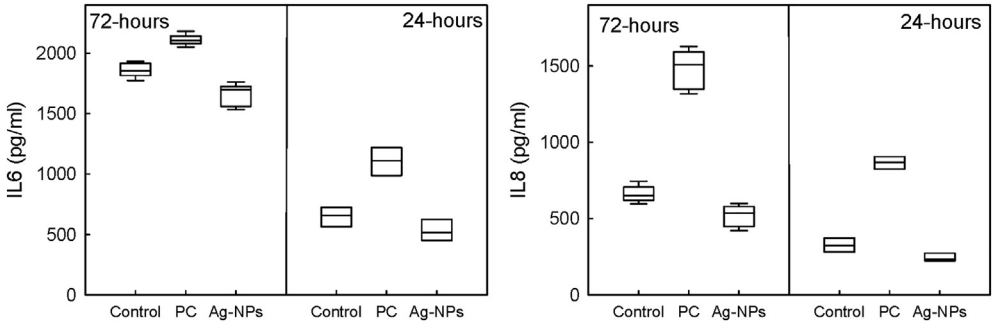


**Fig. 5.** Boxplot of individual IL records. The secretion of IL6 and IL8 of the unexposed cells and the cells exposed to positive control (PC) and 40 μg/ml Ag-NPs for 24 h or 72 h was determined by the ELISA procedures as described in Section 2.12. The nine individual determinations per experimental condition are plotted (3 independent experiments, each with 3 wells) for both IL6 and IL8 after the 72 h exposure, together with the six individual determinations per experimental condition (2 independent experiments, each with 3 wells) for both IL6 and IL8 after the 24 h exposure. PC = Positive control (300 μg/ml of lipopolysaccharides from *Escherichia coli* O55:B5Y).

neuronal cells and during the growth stimulation of glial tumours (Uniprot Database accession number P31371). All this suggests that inappropriate FGF9 performance might also increase the susceptibility of the central nervous system to other insults.

### 4.5. Altered molecular functions: MAPK

Table 4 shows how two different MAPKs activities, specifically "*MAP kinase tyrosine/serine/threonine phosphatase activity*" (GO:0017017) (enrichment factor 84) and "*MAP kinase phosphatase activity*" (GO:0033549) (enrichment factor 77), are overrepresented among the 42 genes with an altered expression as a consequence of exposure to Ag-NPs. Moreover, the inactivation of MAPK activity has also been reported as altered biological process sub-ontology with an enrichment factor of 40 (Table 3). MAPK signalling is widely conserved along the phylogenetic scale for regulating cellular processes such as migration, proliferation, differentiation and death. Two major MAPK pathways are p38 (involved in the cellular response to environmental stress) and ERK (involved in the extracellular signals that direct survival and differentiation) (D'Mello and Chin, 2005). The genes involved in both the negative and positive regulations of cascades ERK1 and ERK2 (enrichment factors 23 and 15, respectively (Table 3)) were found among the biological process overrepresented in the pool of genes with expressions altered by Ag-NPs. The p38 MAPK pathway was identified as an altered molecular pathway after Ag-NPs exposure (Table 5). Thus, T98G cells respond to Ag-NPs insult by altering cellular signalling *via* MAPK, which can induce cellular malfunction.

Table S2 in the Supplementary Material shows the genes that code for several dual specificity protein phosphatases (DUSP). DUSP are powerful regulators of the intensity and duration of MAPK signalling (Pérez-Sen et al., 2019). Specifically, DUSP 4, 5 and 10 were down regulated by 36%, 45% and 40%; respectively (Table S2 in the Supplementary Material). DUSP4 is a phosphatase involved in the regulation of mitogenic signal transduction by dephosphorylating both Thr and Tyr residues in MAP kinases ERK1 and ERK2 (Uniprot Database accession number Q13115). DUSP 5 is a phosphatase that is active with phosphotyrosine with the greatest relative activity towards ERK1 (Uniprot Database accession number Q16690). DUSP 10 is a phosphatase involved in the inactivation of MAP kinases (Uniprot Database accession number Q9Y6W6). Thus, the down-regulation of these genes supports the involvement of MAPK pathways as the main molecular mechanism of response of T98G cells to Ag-NPs insults.

### 4.6. Role of silver ions

Several authors reported that some of the effects associated to Ag-NPs might be partially attributed to or enhanced by soluble silver ions released during exposure (Węsierska et al., 2018; Polet et al., 2020). Silver ions can uncouple enzymes of respiratory chain causing ATP depletion (AshaRani et al., 2009), oxidative stress (Prasad et al., 2013) and inflammation with IL release (Polet et al., 2020). However, it is noted that in our experimental conditions no alterations in cell viability was reported with MTT test; which is a test based on mitochondrial working and thus should have been able to detect reductions in viability due to oxidative stress and uncoupling of respiratory chain proteins. Moreover, no indications of oxidative stress were detected in the RNAseq. By example, no alterations in Nrf-2/ARE (an indicator and modulator of oxidative stress in neurodegeneration (Johnson et al., 2008)) or NFkB (a protein complex involved in cellular response to stimuli such as oxidative stress and cytokines (Moniruzzaman et al., 2018)) were found. Finally, our data show reductions in IL secretion, and not an increase in secretions of these substances, as reported by other authors (Polet et al., 2020). Therefore, we consider that it is highly unlikely that the effects reported in this work might be attributed to soluble silver ions.

### 4.7. Risk

The highest concentration (the upper edge of the 95% confidence interval of the 95th percentile) of Ag circulating in whole blood in the Canadian population has been reported as 0.42 μg/l (42 ng/ml) (Ministry of Health of Canada Government, 2013). By assuming the worst case, that is, all this silver comes in a nanoparticulate form; this silver concentration is 2 orders of magnitude lower than the lowest concentration known to cause a statistically significant alteration in the expression of genes (Fig. 4).

A health surveillance case study with workers who manufacture Ag nanomaterials has provided a report about one male worker exposed for 7 years to 1.35 $\mu g/m^3$ Ag-NPs to present an Ag concentration in blood of 0.0135 μg/dl (0.135 ng/ml) (Lee et al., 2012). This level of Ag circulating in blood is several orders of magnitude lower than the concentrations of concern reported in Fig. 4.

These data suggests that the risk for the above-discussed effects seems low at the current exposure levels noted in the general population. However, exposure in specific applications related to biomedical applications, especially those involving systemic exposure as wound and bone healing, or the use of modified catheters, should be carefully assessed as it might imply a significantly greater exposure than that which the general population is exposed.

## 5. Conclusions

We have characterised the effects of Ag-NPs on T98G human glioblastoma cells following the approach proposed by the National Academy of Sciences, USA (2007), which suggested that toxicology testing in 21st century should evolve towards a new paradigm based on the identification of biologically relevant molecular perturbations caused in (preferably) human cells as a first response to exposure. We have found transcriptomic alterations in several molecular pathways. The meaning of some of these molecular pathways in glia cells is still unclear, but some authors have suggested that the performance of glia cells might be severely affected as a consequence of neuro-inflammation and of FGF pathway and MAPK cascades dysregulation (Ornitz and Itoh, 2015; D'Mello and Chin, 2005). This would eventually lead to neurotoxicity, especially when considering the critical role of glia in synapse formation, function, plasticity and elimination, and in the control of blood flow, blood brain barrier maintenance, and in disease, repair and regeneration of the central nervous system (Barres et al., 2015).

Our data also remarkably suggest that the risk of occurrence of the above-discussed effects is relatively low as effects were detected at concentrations that came very close to the solubility limits and were, in turn, far from the Ag concentration reported in the general population.

## Declaration of Competing Interest

All the authors declare no financial and personal relationships with other people or organizations that could inappropriately influence (bias) this work.

## Acknowledgments

This work was supported by the Ramón Areces Foundation (Grant CIVP18A3939). The sponsor had no role on the study design, collection, interpretation and analysis of data; in the writing of this manuscript; and in the decision to submit the article for publication. Special thanks go to María José López Andreo, José Muñoz Ramos, Antonia Bernabeu Esclapez, Alejandro Torrecillas Sánchez and María García García from ACTI for their kindness and support.

## Appendix A. Supplementary data

Supplementary data to this article can be found online at https://doi.org/10.1016/j.taap.2020.115178.

## References


Amiri, S., Yousefi-Ahmadipour, A., Hosseini, M.J., Haj-Mirzaian, A., Momeny, M., Hosseini-Chegeni, H., Mokhtari, T., Kharrazi, S., Hassanzadeh, G., Amini, S.M., Jafarinejad, S., Ghazi-Khansari, M., 2018. Maternal exposure to silver nanoparticles are associated with behavioral abnormalities in adulthood: role of mitochondria and innate immunity in developmental toxicity. Neurotoxicology 66, 66–77. https://doi.org/10.1016/j.neuro.2018.03.006.

AshaRani, P.V., Low Kah Mun, G., Hande, M.P., Valiyaveettil, S., 2009. Cytotoxicity and genotoxicity of silver nanoparticles in human cells. ACS Nano 3, 279–290. https://doi.org/10.1021/nn800596w.

Ashburner, M., Ball, C.A., Blake, J.A., Botstein, D., Butler, H., Cherry, J.M., Davis, A.P., Dolinski, K., Dwight, S.S., Eppig, J.T., Harris, M.A., Hill, D.P., Issel-Tarver, L., Kasarskis, A., Lewis, S., Matese, J.C., Richardson, J.E., Ringwald, M., Rubin, G.M., Sherlock, G., 2000. Gene ontology: tool for the unification of biology. Nat. Genet. 25, 25–29. https://doi.org/10.1038/75556.

Barres, B.A., Freeman, M.R., Stevens, B., 2015. Glia. Cold Spring Harbor, New York (ISBN: 978-1-62182-027-7).

Begum, A.N., Aguilar, J.S., Elias, L., Hong, Y., 2016. Silver nanoparticles exhibit coating and dose-dependent neurotoxicity in glutamatergic neurons derived from human embryonic stem cells. Neurotoxicology 57, 45–53. https://doi.org/10.1016/j.neuro.2016.08.015.

Bolger, A.M., Lohse, M., Usadel, B., 2014. Trimmomatic: a flexible trimmer for Illumina sequence data. Bioinformatics 30, 2114–2120. https://doi.org/10.1093/bioinformatics/btu170.

Burduşel, A.C., Gherasim, O., Grumezescu, A.M., Mogoantă, L., Ficai, A., Andronescu, E., 2018. Biomedical applications of silver nanoparticles: an up-to-date overview. Nanomaterials (Basel) 8https://doi.org/10.3390/nano8090681. pii: E681.

Coccini, T., Caloni, F., Ramírez Cando, L.J., De Simone, U., 2017. Cytotoxicity and proliferative capacity impairment induced on human brain cell cultures after short- and long-term exposure to magnetite nanoparticles. J. Appl. Toxicol. 37, 361–373. https://doi.org/10.1002/jat.3367.

D'Mello, S.R., Chin, P.C., 2005. Treating neurodegenerative conditions through the understanding of neuronal apoptosis. Curr. Drug Targets CNS Neurol. Disord. 4, 3–23. https://doi.org/10.2174/1568007053005118.

EC (European Commission), 2016. Catalogue of Nanomaterials used in Cosmetic Products placed on the Market. Accessed 11 April 2020. https://ec.europa.eu/docsroom/documents/35411.

Eisen, M.B., Spellman, P.T., Brown, P.O., Botstein, D., 1998. Cluster analysis and display of genome-wide expression patterns. Proc. Natl. Acad. Sci. U. S. A. 95, 14863–14868. https://doi.org/10.1073/pnas.95.25.14863.

Estevan, C., Vilanova, E., Sogorb, M.A., 2013. Chlorpyrifos and its metabolites alter gene expression at non-cytotoxic concentrations in D3 mouse embryonic stem cells under in vitro differentiation: considerations for embryotoxic risk assessment. Toxicol. Lett. 217, 14–22. https://doi.org/10.1016/j.toxlet.2012.11.026.

Estevan, C., Fuster, E., Del Río, E., Pamies, D., Vilanova, E., Sogorb, M.A., 2014. Organophosphorus pesticide chlorpyrifos and its metabolites alter the expression of biomarker genes of differentiation in D3 mouse embryonic stem cells in acomparable way to other model neurodevelopmental toxicants. Chem. Res. Toxicol. 27, 1487–1495. https://doi.org/10.1021/tx500051k.

European Union, 2011. Commission Recommendation of 18 October 2011 on the Definition of Nanomaterial (Accessed 11 April 2020). https://ec.europa.eu/research/industrial_technologies/pdf/policy/commission-recommendation-on-the-definition-of-nanomater-18102011_en.pdf.

European Union Observatory for Nanomaterials (EUON), 2020. Accessed 11 April 2020. https://euon.echa.europa.eu/.

Ghooshchian, M., Khodarahmi, P., Tafvizi, F., 2017. Apoptosis-mediated neurotoxicity and altered gene expression induced by silver nanoparticles. Toxicol. Ind. Health 33, 757–764. https://doi.org/10.1177/0748233717719195.

Gokarneshan, N., Velumani, K., 2017. Application of nano silver particles on textile materials for improvement of antibacterial finishes. Glob. J. Nanomed. 2, 555586. https://doi.org/10.1177/0748233717719195.

Gonzalez-Carter, D.A., Leo, B.F., Ruenraroengsak, P., Chen, S., Goode, A.E., Theodorou, I.G., Chung, K.F., Carzaniga, R., Shaffer, M.S., Dexter, D.T., Ryan, M.P., Porter, A.E., 2017. Silver nanoparticles reduce brain inflammation and related neurotoxicity through induction of H(2)S-synthesizing enzymes. Sci. Rep. 7, 42871. https://doi.org/10.1038/srep42871.

Guo, Y., Dai, Y., Yu, H., Zhao, S., Samuels, D.C., Shyr, Y., 2017. Improvements and impacts of GRCh38 human reference on high throughput sequencing data analysis. Genomics 109, 83–90. https://doi.org/10.1016/j.ygeno.2017.01.005.

Hoyt, B.W., Mason, E., 2008. Nanotechnology emerging health issues. J. Chem. Health Saf. 15, 10–15. https://doi.org/10.1016/j.jchas.2007.07.015.

Johnson, J.A., Johnson, D.A., Kraft, A.D., Calkins, M.J., Jakel, R.J., Vargas, M.R., Chen, P.C., 2008. The Nrf2-ARE pathway: an indicator and modulator of oxidative stress in neurodegeneration. Ann. N. Y. Acad. Sci. 1147, 61–69. https://doi.org/10.1196/annals.1427.036.

Kim, D., Langmead, B., Salzberg, S.L., 2015. HISAT: a fast spliced aligner with low memory requirements. Nat. Methods 12, 357–360. https://doi.org/10.1038/nmeth.3317.

Kroll, A., Pillukat, M.H., Hahn, D., Schnekenburger, J., 2012. Interference of engineered nanoparticles with in vitro toxicity assays. Arch. Toxicol. 86, 1123–1136. https://doi.org/10.1007/s00204-012-0837-z.

Lee, J.H., Mun, J., Park, J.D., Yu, I.J., 2012. A health surveillance case study on workers who manufacture silver nanomaterials. Nanotoxicology 6, 667–669. https://doi.org/10.3109/17435390.2011.600840.

Li, H., Handsaker, B., Wysoker, A., Fennell, T., Ruan, J., Homer, N., Marth, G., Abecasis, G., Durbin, R., 2009. The sequence alignment/map format and SAMtools. Bioinformatics 25, 2078–2079. https://doi.org/10.1093/bioinformatics/btp352.

Luther, E.M., Koehler, Y., Diendorf, J., Epple, M., Dringen, R., 2011. Accumulation of silver nanoparticles by cultured primary brain astrocytes. Nanotechnology 22, 375101. https://doi.org/10.1088/0957-4484/22/37/375101.

Mannerström, M., Zou, J., Toimela, T., Pyykkö, I., Heinonen, T., 2016. The applicability of conventional cytotoxicity assays to predict safety/toxicity of mesoporous silica nanoparticles, silver and gold nanoparticles and multi-walled carbon nanotubes. Toxicol. in Vitro 37, 113–120. https://doi.org/10.1016/j.tiv.2016.09.012.

Migliore, L., Uboldi, C., Di Bucchianico, S., Coppedè, F., 2015. Nanomaterials and neurodegeneration. Environ. Mol. Mutagen. 56, 149–170. https://doi.org/10.1002/em.21931.

Ministry of Health of Canada Government, 2013. SECOND Report on Human Biomonitoring of Environmental Chemicals in Canada. Results of the Canadian Health Measures Survey Cycle 2 (2009–2011). ISBN: 978–1–100-22140-3. (Accessed 11 April 2020). https://www.canada.ca/content/dam/hc-sc/migration/hc-sc/ewh-semt/alt_formats/pdf/pubs/contaminants/chms-ecms-cycle2/chms-ecms-cycle2-eng.pdf.

Moniruzzaman, M., Ghosal, I., Das, D., Chakraborty, S.B., 2018. Melatonin ameliorates H(2)O(2)-induced oxidative stress through modulation of Erk/Akt/NFkB pathway. Biol. Res. 51, 17. https://doi.org/10.1186/s40659-018-0168-5.

Monteiro-Riviere, N.A., Inman, A.O., Zhang, L.W., 2009. Limitations and relative utility of screening assays to assess engineered nanoparticle toxicity in a human cell line. Toxicol. Appl. Pharmacol. 234, 222–235. https://doi.org/10.1016/j.taap.2008.09.030.

Mulvaney, P., Weiss, P.S., 2016. Have nanoscience and nanotechnology delivered? ACS Nano 10, 7225–7226. https://doi.org/10.1021/acsnano.6b05344.

National Academy of Sciences, USA, 2007. Committee on Toxicity Testing and Assessment of Environmental Agents,National Research Council. Toxicity Testing in the 21st Century: A Vision and a Strategy (ISBN: 978-0-309-10992-5 Accessed 11 April 2020). http://nap.edu/11970.

OECD (Organization for Economic Cooperation and Development), 2010. Series on the Safety of Manufactured Nanomaterials No. 27 List of Manufactured Nanomaterials and list of Endpoints for Phase one of the Sponsorship Programme for the Testing of Manufactured Nanomaterials: Revision (Accessed 11 April 2020). http://www.oecd.org/officialdocuments/publicdisplaydocumentpdf/?cote=env/jm/mono(2010)46&doclanguage=en.

Ornitz, D.M., Itoh, N., 2015. The fibroblast growth factor signaling pathway. Wiley Interdiscip. Rev. Dev. Biol. 4, 215–266. https://doi.org/10.1002/wdev.176.

Panossian, A., Seo, E.J., Efferth, T., 2019. Effects of anti-inflammatory and adaptogenic herbal extracts on gene expression of eicosanoids signaling pathways in isolated brain cells. Phytomedicine 60, 152881. https://doi.org/10.1016/j.phymed.2019.152881.

Pérez-Sen, R., Queipo, M.J., Gil-Redondo, J.C., Ortega, F., Gómez-Villafuertes, R., Miras-Portugal, M.T., Delicado, E.G., 2019. Dual-specificity phosphatase regulation in neurons and glial cells. Int. J. Mol. Sci. 20. https://doi.org/10.3390/ijms20081999.

Pertea, M., Kim, D., Pertea, G.M., Leek, J.T., Salzberg, S.L., 2016. Transcript-level expression analysis of RNA-seq experiments with HISAT, StringTie and Ballgown. Nat. Protoc. 11, 1650–1667. https://doi.org/10.1038/nprot.2016.095.

Polet, M., Laloux, L., Cambier, S., Ziebel, J., Gutleb, A.C., Schneider, Y.J., 2020. Soluble silver ions from silver nanoparticles induce a polarised secretion of interleukin-8 in differentiated Caco-2 cells. Toxicol. Lett. 325, 14–24. https://doi.org/10.1016/j.toxlet.2020.02.004.

Powers, K.W., Palazuelos, M., Moudgil, B.M., Roberts, S.M., 2007. Characterization of the size, shape, and state of dispersion of nanoparticles for toxicological studies. Nanotoxicology 1, 42–51. https://doi.org/10.1080/17435390701314902.

Prasad, R.Y., McGee, J.K., Killius, M.G., Suarez, D.A., Blackman, C.F., DeMarini, D.M., Simmons, S.O., 2013. Investigating oxidative stress and inflammatory responses elicited by silver nanoparticles using high-throughput reporter genes in HepG2 cells: effect of size, surface coating, and intracellular uptake. Toxicol. in Vitro 27, 2013–2021. https://doi.org/10.1016/j.tiv.2013.07.005.

Repar, N., Li, H., Aguilar, J.S., Li, Q.Q., Drobne, D., Hong, Y., 2018. Silver nanoparticles induce neurotoxicity in a human embryonic stem cell-derived neuron and astrocyte network. Nanotoxicology 12, 104–116. https://doi.org/10.1080/17435390.2018.1425497.

Rezvani, E., Rafferty, A., McGuinness, C., Kennedy, J., 2019. Adverse effects of nanosilver on human health and the environment. Acta Biomater. 94, 145–159. https://doi.org/10.1016/j.actbio.2019.05.042.

Rose-John, S., 2018. Interleukin-6 Family Cytokines. Cold Spring Harb. Perspect. Biol. 10https://doi.org/10.1101/cshperspect.a028415. pii: a028415.

Saldanha, A.J., 2004. Java Treeview–extensible visualization of microarray data. Bioinformatics 20, 3246–3248. https://doi.org/10.1093/bioinformatics/bth349.

Schmittgen, T.D., Livak, K.J., 2008. Analyzing real-time PCR data by the comparative C(T) method. Nat. Protoc. 3, 1101–11108. https://doi.org/10.1038/nprot.2008.73.

Schulze, C., Schulze, C., Kroll, A., Schulze, C., Kroll, A., Lehr, C.M., Schäfer, U.F., Becker, K., Schnekenburger, J., Schulze-Isfort, C., Landsiedel, R., Wohlleben, W., 2008. Not ready to use-overcoming pitfalls when dispersing nanoparticles in physiological media. Nanotoxicology 2, 51–61. https://doi.org/10.1080/17435390802018378.

Stein, G.H., 1979. T98G: an anchorage-independent human tumor cell line that exhibits stationary phase G1 arrest in vitro. J. Cell. Physiol. 99, 43–54. https://doi.org/10.

1002/jcp.1040990107.
Strużyńska, L., Skalska, J., 2018. Mechanisms underlying neurotoxicity of silver nanoparticles. Adv. Exp. Med. Biol. 1048, 227–250. https://doi.org/10.1007/978-3-319-72041-8_14.
Tanaka, T., Narazaki, M., Kishimoto, T., 2014. IL-6 in inflammation, immunity, and disease. Cold Spring Harb. Perspect. Biol. 6, a016295. https://doi.org/10.1101/cshperspect.a016295.
The Gene Ontology Consortium, 2017. Expansion of the gene ontology knowledgebase and resources. Nucleic Acids Res. 45 (D1), D331–D338. https://doi.org/10.1093/nar/gkw1108.
Trapnell, C., Williams, B.A., Pertea, G., Mortazavi, A., Kwan, G., van Baren, M.J., Salzberg, S.L., Wold, B.J., Pachter, L., 2010. Transcript assembly and quantification by RNA-Seq reveals unannotated transcripts and isoform switching during cell differentiation. Nat. Biotechnol. 28, 511–515. https://doi.org/10.1038/nbt.1621.
Trapnell, C., Roberts, A., Goff, L., Pertea, G., Kim, D., Kelley, D.R., Pimentel, H., Salzberg, S.L., Rinn, J.L., Pachter, L., 2012. Differential gene and transcript expression analysis of RNA-seq experiments with TopHat and cufflinks. Nat. Protoc. 7, 562–578. https://doi.org/10.1038/nprot.2012.016.
Uniprot database accession number O43597, 2020. Protein sprouty homolog 2 entry (SPRY2) (Accessed 11 April 2020). https://www.uniprot.org/uniprot/O43597.
Uniprot database accession number P18146, 2020. Early Growth Response Protein 1 (P18146) (Accessed 11 April 2020). https://www.uniprot.org/uniprot/P18146.
Uniprot database accession number P30414, 2020. NK-Tumor Recognition Protein (P30414) (Accessed 11 April 2020). https://www.uniprot.org/uniprot/P30414.
Uniprot database accession number P31371, 2020. Fibroblast Growth Factor 9 (FGF9) (Accessed 11 April 2020). https://www.uniprot.org/uniprot/P31371.
Uniprot database accession number Q13115, 2020. Dual Specificity Protein Phosphatase 4 (DUSP4) (Accessed 11 April 2020). https://www.uniprot.org/uniprot/Q13115.
Uniprot database accession number Q16690, 2020. Dual Specificity Protein Phosphatase 5 (DUSP5) (Accessed 11 April 2020). https://www.uniprot.org/uniprot/Q16690.
Uniprot database accession number Q9C004, 2020. Protein Sprouty Homolog 4 Entry (SPRY4) (Accessed 11 April 2020). https://www.uniprot.org/uniprot/Q9C004.
Uniprot database accession number Q9Y6W6, 2020. Dual Specificity Protein Phosphatase 10 (DUSP10) (Accessed 11 April 2020). https://www.uniprot.org/uniprot/Q9Y6W6.
Vance, M.E., Kuiken, T., Vejerano, E.P., McGinnis, S.P., Hochella Jr., M.F., Rejeski, D., Hull, M.S., 2015. Nanotechnology in the real world: redeveloping the nanomaterial consumer products inventory. Beilstein J. Nanotechnol. 6, 1769–1780. https://doi.org/10.3762/bjnano.6.
Węsierska, M., Dziendzikowska, K., Gromadzka-Ostrowska, J., Dudek, J., Polkowska-Motrenko, H., Audinot, J.N., Gutleb, A.C., Lankoff, A., Kruszewski, M., 2018. Silver ions are responsible for memory impairment induced by oral administration of silver nanoparticles. Toxicol. Lett. 290, 133–144. https://doi.org/10.1016/j.toxlet.2018.03.019.
Zhang, Y., Chen, Y., Westerhoff, P., Hristovski, K., Crittenden, J.C., 2008. Stability of commercial metal oxide nanoparticles in water. Water Res. 42, 2204–2212. https://doi.org/10.1016/j.watres.2007.11.036.
Zucker, R.M., Daniel, K.M., 2012. Detection of TiO2 nanoparticles in cells by flow cytometry. Methods Mol. Biol. 906, 497–509. https://doi.org/10.1007/978-1-61779-953-2_40.
Zucker, R.M., Massaro, E.J., Sanders, K.M., Degn, L.L., Boyes, W.K., 2010. Detection of TiO2 nanoparticles in cells by flow cytometry. Cytometry A 77, 677–685. https://doi.org/10.1002/cyto.a.20927.
Zucker, R.M., Ortenzio, J.N., Boyes, W.K., 2016. Characterization, detection, and counting of metal nanoparticles using flow cytometry. Cytometry A 89, 169–183. https://doi.org/10.1002/cyto.a.22793.